4

# SOLID STATE DIFFUSION IN $PD_2SI$

by

JOHN MATHEW EGAN



Dissertation presented to the
University of Cape Town
in fulfilment of the requirements
for the degree of

MASTER OF SCIENCE

Department of Physics
University of Cape Town

October 1986

## ABSTRACT

The atomic transport processes ocurring in the Pd/Si system have been investigated. The $Pd_2Si$ system has been studied to try and establish the mechanism(s) of diffusion by which the growth of $Pd_2Si$ proceeds under thermal annealing.

Using a deposited Ti marker, the dominant moving species during $Pd_2Si$ formation in the temperature range 250-400°C has been determined to be silicon. Palladium transport appears to occur during the initial stages of formation of $Pd_2Si$. Once several hundred angstrom of $Pd_2Si$ has been formed, palladium transport seems to be replaced by silicon transport.

Silicon tracer experiments, in conjunction with Si self-diffusion measurements, indicate that silicon mobility is exceptionally high during the formation of $Pd_2Si$ on Si<a> substrate. During growth, the mobility of silicon is orders of magnitude higher than under equilibrium conditions. This is thought to suggest a vacancy mechanism of diffusion, and is expected that large numbers of vacancies are generated at the growth interface during silicide formation.

Silicon self-diffusion in $Pd_2Si$ has been investigated. The results indicate that grain-boundary diffusion could be operative under equilibrium conditions. Under the assumption that grain-boundary diffusion does occur during thermal annealing in the range 350-550°C, it is deduced that at all times the grain-boundary diffusivity is so much greater than the lattice diffusivity, that the grain-boundaries are effectively able to act as sources for the grains. The activation energy for lattice self-diffusion of silicon in $Pd_2Si$ which has grown on Si<100> substrate, has been determined to be 0.8±0.3eV. This value is thought to support recent kinetic results which indicate that the activation energy for growth of $Pd_2Si$ is in the region of 1eV.

## ACKNOWLEDGEMENTS

I would like to express my appreciation to following people:

Dr. Craig Comrie, my mentor, Physics department, University of Cape Town, for his guidance, support and friendship;

Dr. R. Pretorius, Ion-solid Interaction Division, Van de Graaff Group, National Accelerator Centre, for his support and interest in the project;

The Director and staff at the Van de Graaf Group, National Accelerator Centre, for use of the facilities;

The Council for Scientific and Industrial Research, for a post-graduate bursary;

The Parish Council, St Mary's Cathedral, Kimberley, for financial assistance;

Madi Pearce, for love and encouragement and for graphic assistance;

Alison Pearce, for graphic assistance;

Colleagues and friends at UCT, SUNI, KHANYA, and Osborne Road, for their continuous support and encouragement;

my parents, for their love and support;

*for my family*

CONTENTS


1. Introduction 1
   1.1 Introduction
   1.2 Markers
   1.2.1 Implantation
   1.2.2 Deposited markers
   1.2.3 Radioactive markers
   1.3 Diffusion
   1.3.1 Introduction
   1.3.2 Mathematical formulation and solution
   1.3.3 Grain-boundary diffusion
   1.3.4 Diffusion controlled growth

2. Experimental 23
   2.1.1 Sample preparation and deposition
   2.1.2 Evaporation
   2.2 Thermal annealing
   2.3 Rf sputtering
   2.4 Rutherford backscattering spectrometry

3. Determination of the dominant moving species 37
   3.1 Introduction
   3.2 Experimental
   3.3 Results
   3.4 Discussion

4. Radioactive silicon tracer experiment 51
   4.1 Introduction
   4.2 Experimental
   4.3 Results
   4.4 Discussion

5. Silicon self-diffusion in $Pd_2Si$ 65
   5.1 Introduction
   5.2 Experimental
   5.3 Results
   5.4 Discussion

6. Conclusion 83

7. Appendix: Coupled grain-boundary lattice diffusion model 90

8. References 108

# CHAPTER ONE

## 1.1 Introduction

Metal silicides have found widespread application in the fabrication of integrated circuits. Their usefulness as ohmic contacts and Schottky barriers has been firmly established [ 1, 2 ]. In fig. 1 the fabrication of a contact is illustrated. Initially an $SiO_2$ layer is grown from the p-type silicon which forms part of the p-n junction. The oxide layer is then etched to expose a window to the p-type silicon. A layer of metal -in this case Pt- is then evaporated onto the underlying silicon. Upon thermal annealing of this structure, the Si and Pt react to form a stable conducting material, $Pt_2Si$ which is then in intimate contact with the p-n junction and therefore with the environment external to the semiconductor device. As device sizes continue to shrink still further, the microelectronics technology has demanded a better understanding of the mechanical, electrical and morphological properties of these materials.

Metal silicides result when metal and silicon layers react via a solid-solid interaction at elevated temperatures. Usually, thin film silicides are comprised of single discrete phases, i.e. the simultaneous formation of different phases is quite uncommon [ 1, 3, 4 ]. Generally, the first phase to form in an M-Si

couple is the metal rich silicide, $M_2Si$. This is followed typically by the formation of silicide phases which become progressively more silicon rich.

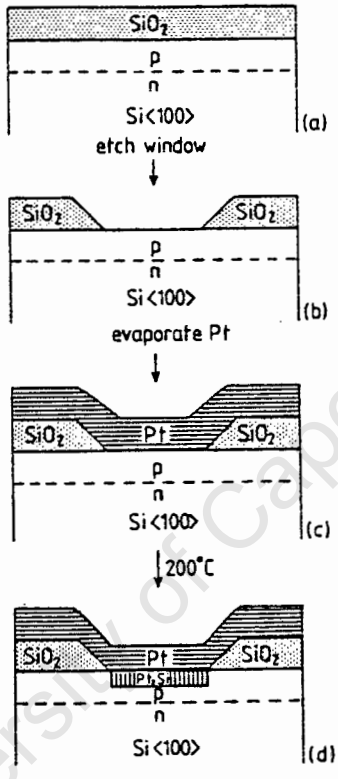


Fig. 1.1 Production of a silicide used as an ohmic or rectifying contact in an integrated circuit.

(a) A silicon wafer containing a p-n junction is oxidized to form a thin $SiO_2$ layer.

(b) A window is etched in the $SiO_2$.

(c) Pt is evaporated over this structure.

(d) Annealing at 200°C forms $Pt_2Si$.

The system investigated in this work, the palladium silicon thin film system, usually only has 2 stable phases viz. the metal rich phase, $Pd_2Si$, and the monosilicide phase, PdSi. In the Pd-Si system the formation of the first phase, $Pd_2Si$, occurs at temperatures above 200 °C. The existence of the phase $Pd_3Si$ has been reported for silicide grown on silicon substrate, but is generally not present to any measurable extent [ 5 ].

Onset of the formation of the monosilicide is reported to occur at the exceptionally high temperature of 810 °C, whereafter growth of that phase proceeds with great rapidity [ 6 ]. The high temperature of monosilicide formation is unusual, as other transition metal silicides transform to the monosilicide at temperatures typically in the region of 400 °C [ 8, 9 ].



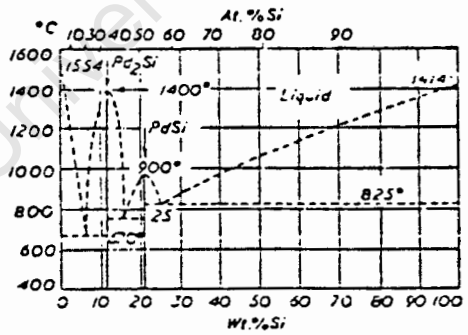


Pd-Si

Fig. 1.2 The phase diagram of the Pd-Si system [ 12 ].

The structure of PdSi formed by thermal annealing at temperatures around 850 $^{o}$C is found to be laterally non-uniform and the existence of island like structures has been reported [ 10 ]. The observation of disjoint islands of PdSi together with the sudden, rapid formation of the phase is taken to imply that the initiation of second phase growth is nucleation controlled and that the nucleation barrier can only be overcome at high temperatures [ 11, 12 ]. Further support for the nucleation barrier hypothesis has come from experiments where it has been reported that low temperature formation of PdSi can be initiated after 300 keV $Ar^{+}$ ion implantation of $Pd_2Si$ layers to form a thin PdSi film at the Si/$Pd_2Si$ interface, followed by 350 $^{o}$C thermal annealing [ 12 ]. It is thought that the amorphorization of the silicon by the implanted ions lowers the nucleation barrier. On the other hand, it has been shown that in the presence of excess Si, the reverse transformation :

$$PdSi \rightarrow Pd_2Si$$

occurs if PdSi is annealed below 800$^{o}$C [ 15 ]. This anomalous behaviour has recently been interpreted as due to the eutectoid decomposition of PdSi at 824 $^{o}$C,( see fig. 1.2 ), as opposed to the earlier suggestion that the lower interfacial energy of the $Pd_2Si$-Si interface was responsible for the reversible phase transformation [ 16 ].

The first phase, $Pd_2Si$, has a hexagonal crystal lattice structure with a basic unit cell comprising 288 atoms. The crystallographic parameters are 13.055Å for the a-axis and 27.490Å for the c-axis [ 17 ].

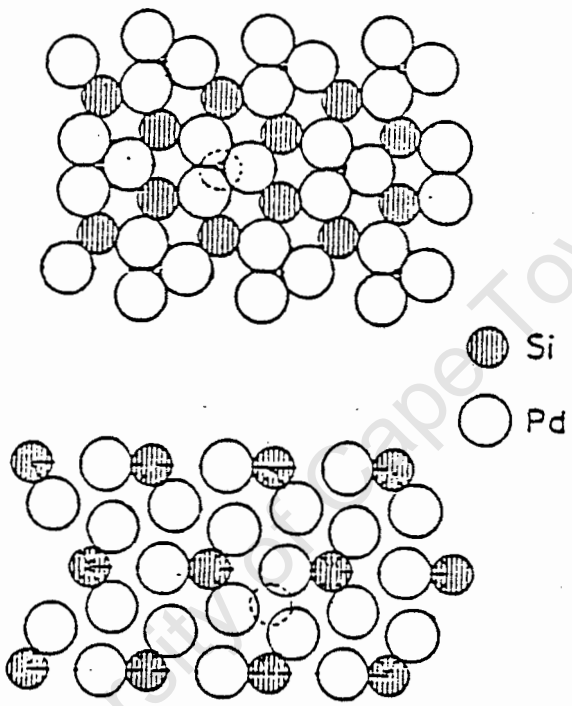




Fig. 1.3 The $Pd_2Si$ structure normal to the c-axis is comprised of two alternating planes. The $a_1$ and $a_2$ unit cell vectors are both 6.53 Å. The two figures represent alternating atomic planes The dotted circles indicate the position of a Si atom in the plane above or the plane below.

$Pd_2Si$ grown on either Si<100> or amorphous silicon substrate is comprised of numerous polycrystals. It is found that the average size of the polycrystals of $Pd_2Si$ formed on amorphous silicon is from 50-300Å [ 18, 19 ], while for silicide grown on Si<100> substrate, the average grain size is in the range 100-800Å . Zingu has found evidence that grain size is proportional to the silicide film thickness [ 20 ]. The grains are found to be oriented randomly with respect to the a-axis for $Pd_2Si$ grown on an amorphous substrate and in the case of $Pd_2Si$ grown on Si<100>, the basal plane is observed to be parallel to the substrate surface. Similar growth with the basal plane parallel to the substrate has been reported for $Pd_2Si$ grown on Si<111>. The silicide grown on this substrate is epitaxial and numerous workers have reported that the angular spread of crystallites in the silicide is only $\sim 1^{\circ}$, implying that the silicide has very low angle grain boundaries [ 21, 22, 23, 24 ]. A temperature dependence of the degree of epitaxy has been reported, and it is found that high temperature formation of the silicide enhances the degree of epitaxy and lowers the angular spread of crystallite orientation [ 23 ]. Typical grain size for $Pd_2Si$ grown on Si<111> substrate is reported to be in the range 200-800Å [ 18 ].

The formation of $Pd_2Si$ occurs in the range 200-700 $^{\circ}C$ and the growth kinetics have been found to be dependent on $\sqrt{t}$. This behaviour is characteristic of a growth process where the transport of material to the growth interface(s) is the rate

controlling feature. Kinetic data of the growth of $Pd_2Si$ for a variety of substrates, have been obtained by numerous authors [ 10, 18 , 24, 25, 26, 27 ], and the activation energy of formation has been determined to be from 0.9-1.5 eV. Most values of the activation energy are around 1.3 eV with the notable exceptions of 1.06eV obtained by Coulman et al [ 66 ] for $Pd_2Si$ grown on Si<111> substrate and 0.9-1.05 eV obtained by Cheung et al [ 18 ] for silicide grown on a variety of substrates. These authors also report that the growth rate of $Pd_2Si$ is most rapid when grown on amorphous silicon substrate, followed by Si<100> and Si<111> grown $Pd_2Si$ respectively. $Pd_2Si$ is found to grow laterally parallel to the substrate surface but, although the interfaces are quite uniform, it has been reported that the Si-$Pd_2Si$ and the Pd-$Pd_2Si$ interfaces may exhibit interfacial roughness of up to 500Å. [ 28, 29 ]. Interfacial roughness at the Si-$Pd_2Si$ interface has been interpreted as due to oxygen contamination, while interfacial voids along the Pd-$Pd_2Si$ contact region are thought to be indicative of a flux of palladium atoms through the silicide, presumably as a result of palladium participation as a diffusing species [ 29 ].

The question of the flux of atoms during the growth of $Pd_2Si$ has remained uncertain for many years. The confusion has resulted from the apparent participation of both silicon and palladium transport in the growth process. The growth of metal rich silicides is usually found to be limited by the supply of metal

atoms to the growth interface [ 30, 31, 32 ]. It has been sufficient to use the term "moving species" when describing that element whose flux is responsible for controlling the growth of the silicide. Since it appears that both palladium and silicon transport is non-negligible during the growth of $Pd_2Si$, the term "dominant moving species", (DMS), is now more appropriate for $Pd_2Si$ to describe that species which limits the growth rate of the silicide, since it appears that both palladium and silicon transport are non-negligible during the growth of $Pd_2Si$.

Earliest work on determining the DMS during $Pd_2Si$ formation was carried out using the technique of inert markers. Chu et al [ 32 ], using implanted $Ar^+$ markers, concluded that both Si and Pd are responsible for controlling the growth of thermally grown $Pd_2Si$. Pretorius et al [ 34, 35 ] conclude that both Pd and Si are diffusing species based on work performed using radioactive $^{31}Si$ as a tracer. That both Pd and Si diffuse appreciably during the formation of the silicide has been reported by other authors; Cheung et al [ 18 ] have interpreted the presence of interfacial voids at the Pd-$Pd_2Si$ and at the Si-$Pd_2Si$ interfaces as suggestive of the dual diffusion of Pd and Si. Foll et al [ 29 ], examining the movement of interfacial oxide agree with the hypothesis. On the basis of inert Ti and W marker movement, Ho et al [ 36 ] have suggested that silicon is the dominant diffusing species once the unimpeded flux of silicon is assured. They conclude, in agreement with Scott et al [ 37 ], that palladium is only mobile during the initial stages of silicide

formation when the interfacial oxide barrier has to be overcome. This reaction is ostensibly responsible for the non-parabolic growth rate during the initial stages of silicide formation. The reduction in growth rate may even be so severe that the reaction appears to halt, giving rise to the so called "incubation period". Scott has suggested that the palladium dissolves the oxide during the early stages, and that it is this which gives rise to the apparent motion of palladium during the growth. Utilizing the epitaxial structure of $Pd_2Si$ grown on Si<111>, Lien et al [ 38 ] conclude that palladium is the dominant diffusing species when diffusion to the growth interface has to occur through epitaxial $Pd_2Si$. Hung and Mayer [ 39 ] have used deposited inert markers to conclude that both Pd and Si are diffusing species during $Pd_2Si$ growth, with palladium being the dominant diffusing species.

## 1.2 Markers

As indicated above, the most popular approach to determine the extent of involvement of each of the 2 components in the growth process is through the use of inert markers. In particular, the use of deposited inert markers has been extensively adopted as a method of establishing the dominant moving species during silicide growth in thin film M/Si couples. A deposited inert marker is essentially a minute but detectable structure which is introduced into the sample under the premise that it provides a reference frame which is unaffected by events occurring during

the growth process. In a structure such as that illustrated in fig. 1.4, it can be seen that the position of the deposited marker relative to the surface of the sample will vary with that species whose transport provides material for the growth of the new phase. It can be seen, for example, that if silicon is diffusing through the intermediate silicide layer to react at the MSi/M interface, then the amount of material on the right hand side of the marker in the figure will increase as more silicon diffuses past the inert marker. Conversely, if the metal is the component with the larger flux, then the amount of metal on the right hand side of the marker will diminish as the reaction proceeds. The two limiting cases are thus that the marker should be either at or near the surface of the sample, indicating that metal is the moving species, or that the marker should be buried under the total amount of silicide. In the case of $Pd_2Si$, it is found that a situation intermediate to the two limiting cases is observed, indicating that both silicon and metal transport occurs during the formation of this phase. Comparison of the relative motion of the marker with respect to the free surface with movement of the growth interface enables the relative contribution by the individual fluxes to the growth of the silicide phase to be determined. The introduction of a foreign atomic structure ( in the sense that the atoms are chemically different as well as crystallographically ) into the couple has to satisfy a number of important criteria before it can be considered suitable as an inert marker, viz.

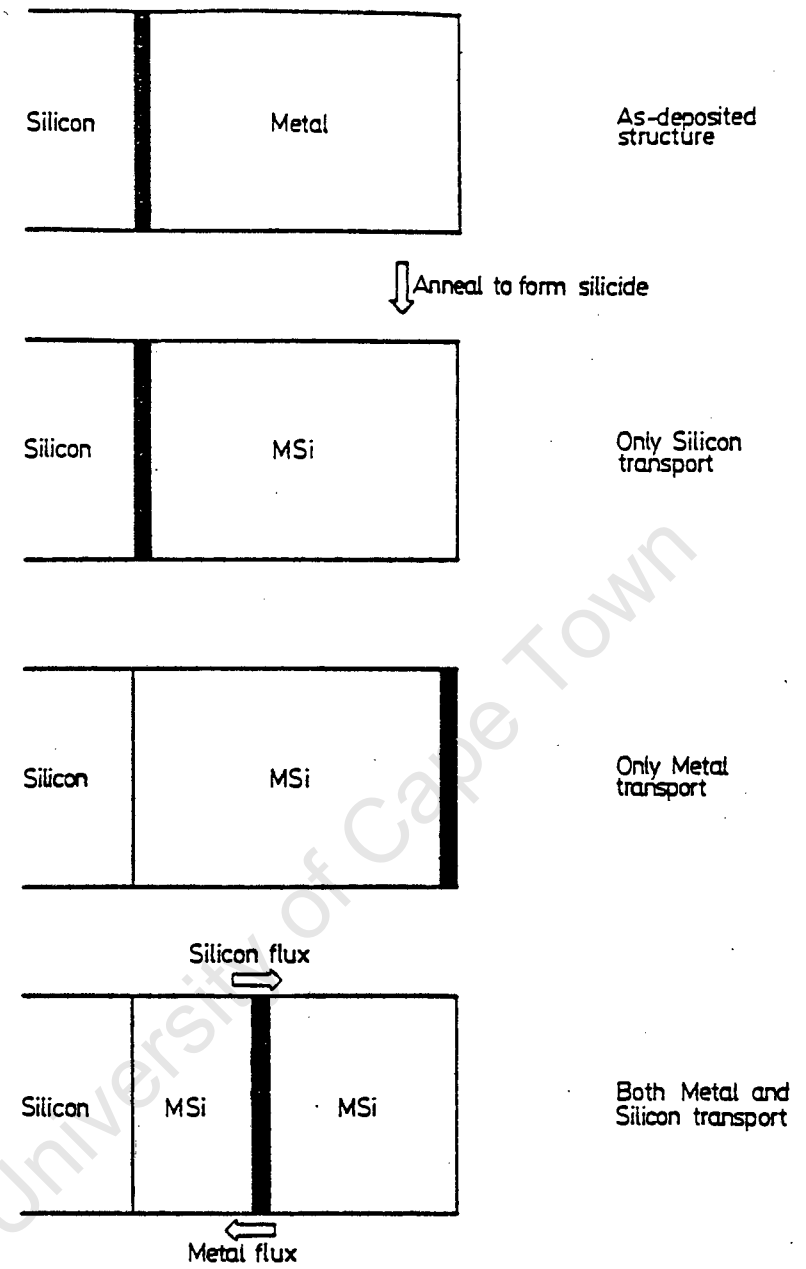




Fig. 1.4 A schematic diagram of the motion of a deposited marker, illustrating the displacement of the marker according to whether the metal or silicon is the diffusing species.

(i) The marker should be chemically inert with respect to the initial components as well as to the final silicide, i.e the marker should not form additional phases with either the initial constituents or the final product.

(ii) The marker should not obstruct or inhibit the natural motion of atoms or interfaces in the system. This leads to the requirement that the deposited marker should constitute only a very thin layer which should be laterally discontinuous i.e. the surface coverage should constitute but a small fraction of the total cross sectional area of the sample.

(iii) Wherever possible, the marker should not be located at or near the initial metal-silicon interface as it is believed that a moving interface may push or drag the marker as it advances.

(iv) The marker should, in addition, be immobile with respect to some external reference frame. This requirement is usually relaxed by permitting marker spreading as long as it is symmetrical.

Inert markers were first used by Kirkendal and Smigelskas [ 40, 41 ], who deposited Mo wires into a copper - zinc couple. By determining the position of the wires before and after interdiffusion, it was concluded that more Zn atoms than Cu had moved past the Mo wires. This has been taken to imply that the

dominant diffusing species during the interaction between copper and zinc is zinc. For thin films, implantation of thin wires is obviously an unfeasible proposition, since the dimensions of the couple are orders of magnitude smaller than in the case of the experiment of Kirkendal et al, and alternate marker methods have been developed.

### 1.2.1 Implantation

Argon atoms have been ion beam implanted for use as a marker by Chu et al [ 42 ]. Since the concentration of argon is low and because argon is chemically inert it is expected that the presence of these gas atoms will not significantly impede the motion of the diffusing metal or silicon atoms. Extensive use has been made of argon as a marker and results obtained from these experiments are in good agreement with results obtained by other means.



### 1.2.2 Deposited markers

In this case, inert metals have been deposited such that they become buried within the region of interest. Van Gurp et al [ 43 ] have used tungsten as a marker to trace the motion of Ni atoms during the formation of NiSi. The analysis of marker motion in bulk samples to determine the interdiffusion coefficient has been developed by Darken [ 44 ] and Kidson [ 45 ].

### 1.2.3 Radioactive markers

Pretorius et al [ 46, 47 ] have made extensive use of radioactive silicon as a marker. Botha [ 47 ] has formulated a computer model to interpret radiotracer experiments investigating diffusion during the solid-solid silicide formation reaction. Figure 1.5 illustrates the basic concept underlying the use of radioactive markers. In the technique, a thin layer of radioactive $^{31}Si$ is deposited onto the silicon substrate. This radioactive $^{31}Si$ layer then reacts with a deposited metal layer. Depending on the the diffusing species and on the mechanism of transport, different final distributions of $M_2{}^{31}Si$ result. If, for example, silicon is the diffusing species and diffuses by a lattice diffusion mechanism, then the final distribution of $^{31}Si$ should be well represented by the illustration in fig. 1.5(b). If on the other hand, the silicon diffuses via a grain-boundary mechanism, then it is expected that, to a good approximation, the $^{31}Si$ which has been incorporated into the silicide should remain relatively inert, while free silicon diffuses past to react with metal at the $M/M_2Si$ interface (fig. 1.5(a)). If metal is the diffusing species, then irrespective of the transport mechanism, the $^{31}Si$ should all be located at the free surface of the silicide. Therefore, a final distribution of of radioactive silicon at the free surface could arise either because of silicon transport via

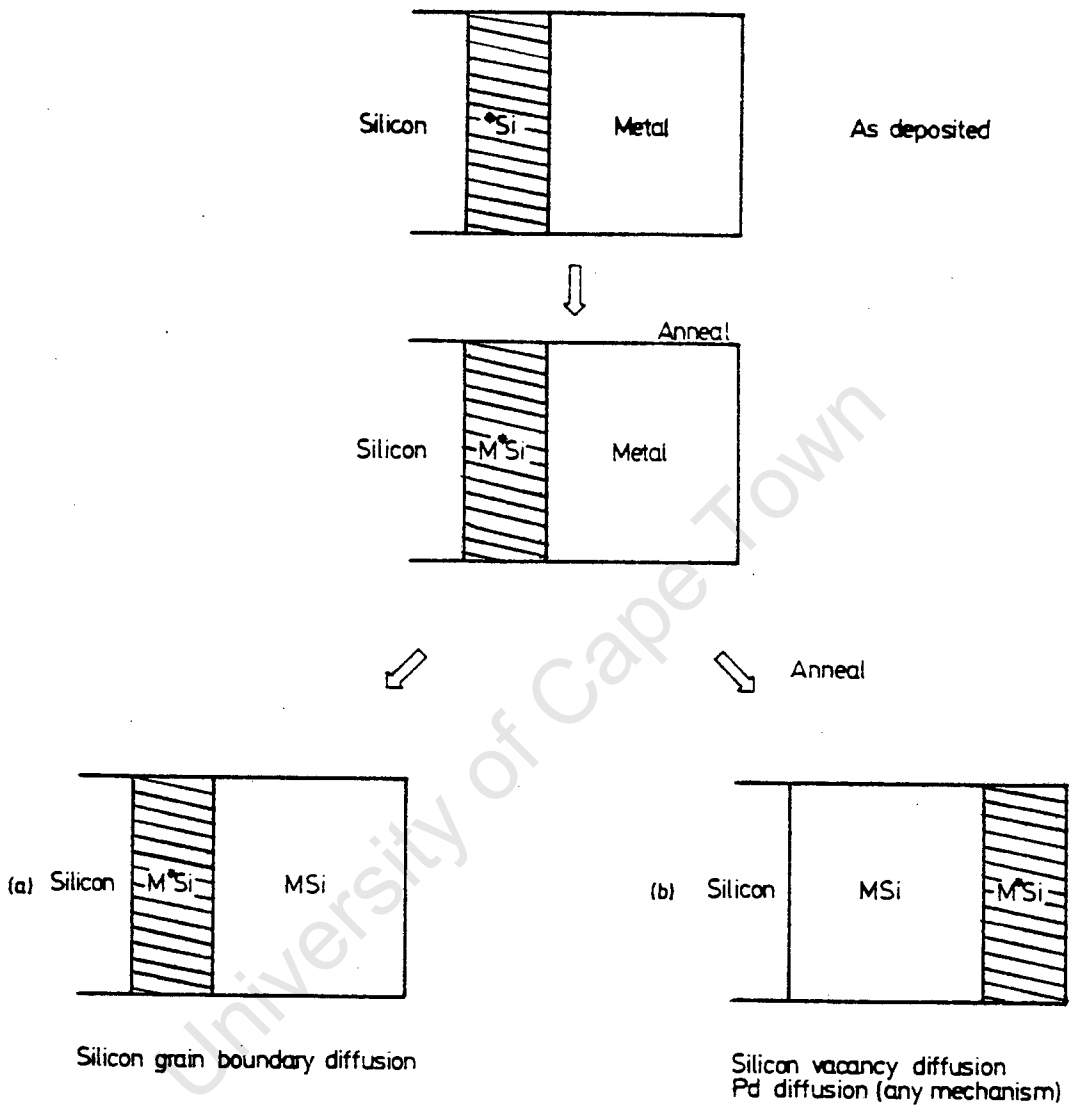




Fig. 1.5 The use of radioactive silicon in determining the transport mechanism during the first phase formation of a silicide.

a vacancy mechanism or metal transport by a vacancy or a grain-boundary mechanism. Results obtained by Botha et al have generally been in good agreement with other work, and it has been possible to establish metal diffusion as the rate controlling mechanism during the formation of various silicides. It has been pointed out, by Ho et al [ 63 ], that the use of a radioactive marker is, in itself, not sufficient to establish unambiguously the dominant moving species during the formation of metal silicides. These authors emphasize that radioactive marker results must be supplemented by inert marker results in order that the DMS determination be unambiguous.

Lien [ 64 ] has extended the model of botha by explicitly considering the atomic defect concentration which gives rise to the diffusion mechanism. The results of this work show that in practice the profiles would not be as sharply defined as predicted by the Botha model. The presence of defects is expected to give rise to a broadening or spreading of the radioactive silicon tracer profiles. In particular, they point out that a completely flat profile could result from a high self-diffusivity of silicon in the silicide irrespective of the transport mechanism.

## 1.3 Diffusion

### 1.3.1. Introduction

The diffusion of atoms is defined to be that atomistic process whereby the random thermal motions of constituent atoms on a crystal lattice give rise to a macroscopic transport of matter in the crystal. Numerous possible mechanisms whereby atoms can move about the crystal have been postulated [ 48 ]. The transference of an atom is favoured when a mobile imperfection is present at a site adjacent to that atom. For example, in fig. 1.6, atom-vacancy exchanges result in the movement of an atom from one site to another. In the classical approach, it is proposed that a certain energy barrier has to be overcome in order that an atom at a given position move to an alternate lattice or interstitial site. The probability and rate with which an atom undergoes a change of position can be related, using a Boltzmann statistical approach, to the so-called activation energy of that process. Atoms are assumed to undergo some form of random walk on the crystal lattice and an analysis of this yields the result that the net displacement of an atom is proportional to the square root of the time over which the displacement has occurred.

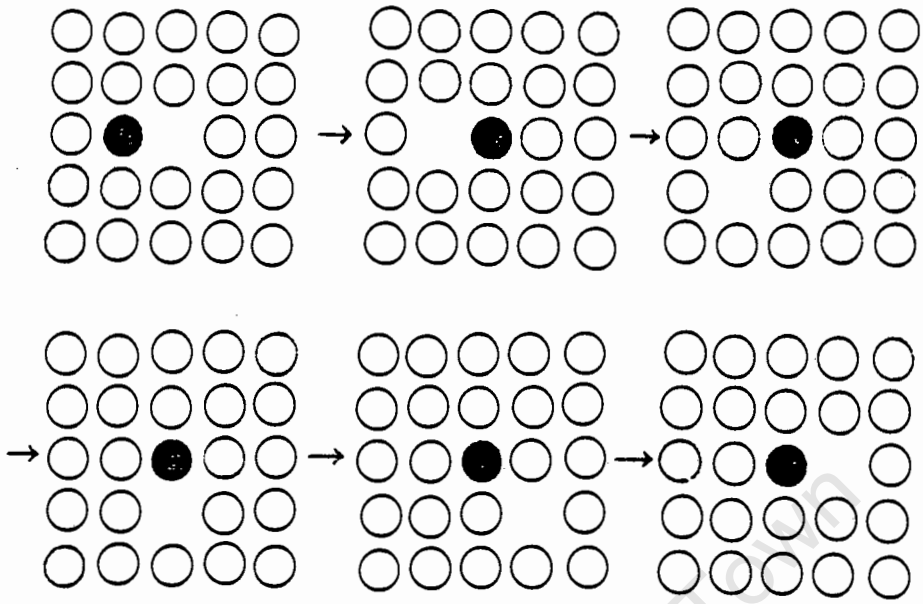

Fig. 1.6 The displacement of a marked atom via atom-vacancy exchanges is illustrated.



1.3.2. Mathematical formulation and solution

Starting from an atomistic model of the process, it is possible to arrive at a description which is approximate to the continuum description of diffusion. In the continuum formulation, diffusion is described by Fick's Laws :

(i) The flux of diffusing atoms across a given plane is proportional to the concentration gradient of that species across the plane.

(ii) The time rate of change of concentration of a species across a given plane is proportional to the flux gradient of that species across the given plane.

These two laws can be summarized by the non-linear equation:

$$\frac{\partial C}{\partial t} = \frac{\partial}{\partial x}\left(-D \frac{\partial C}{\partial x}\right) \qquad [\ 1\ ]$$

where C = C(x,t) is the concentration as a function of position and of time and D is the diffusion coefficient. Usually, D is assumed to be independent of position and time and this yields the linear form of Fick's $2^{nd}$ law:

$$\frac{\partial C}{\partial t} = -D\frac{\partial^2 C}{\partial x^2} \qquad [\ 2\ ]$$

The solution of this equation is subject to the particular boundary conditions. The problem of interest to thin film workers is that of a finite region with a finite source of diffusant at one end of the sample. A thin source of tracer atoms is located at the front surface of the sample. It is assumed that all edges of the crystal are perfectly reflecting and that there is no net flux of the diffusing species across these surfaces. Using these assumptions and considering 1-D diffusion, it can be shown that the concentration of tracer atoms at some distance x and at time t, is given by :

$$\frac{1}{2}C_o \sum_{n=-\infty}^{\infty} \left\{ \operatorname{erf} \frac{h+2nl-x}{2\sqrt{(Dt)}} + \operatorname{erf} \frac{h-2nl+x}{2\sqrt{(Dt)}} \right\}$$

where $C_o$ is the initial tracer concentration in the source region, h is the source thickness and l is the total thickness of the film.

1.3.3. Grain-boundary diffusion

Turnbull and Hoffman [ 50 ] have reported that self-diffusion of radioactive silver is found to be more rapid in polycrystalline silver than in single crystals. This has been interpreted as being due to so-called grain boundary diffusion. Fisher [ 51 ] has modelled the situation in which it is supposed that the grain boundary can be thought of as a thin slab of high diffusivity material imbedded in a matrix of material which has a much lower diffusivity. The Fisher model has been improved upon by Whipple [ 52 ] who, using a method involving Fourier Laplace transforms, has analytically solved the diffusion equations for the case of 2-dimensional diffusion into a semi-infinite sample, assuming that the source is kept constant throughout the diffusion anneal. In the Whipple solution, it is assumed that the concentration variation across a grain boundary can be reasonably approximated by a parabolic even function. Austin and Richards [ 53 ] have investigated the diffusion of gold into copper using thick and thin sources. Electron

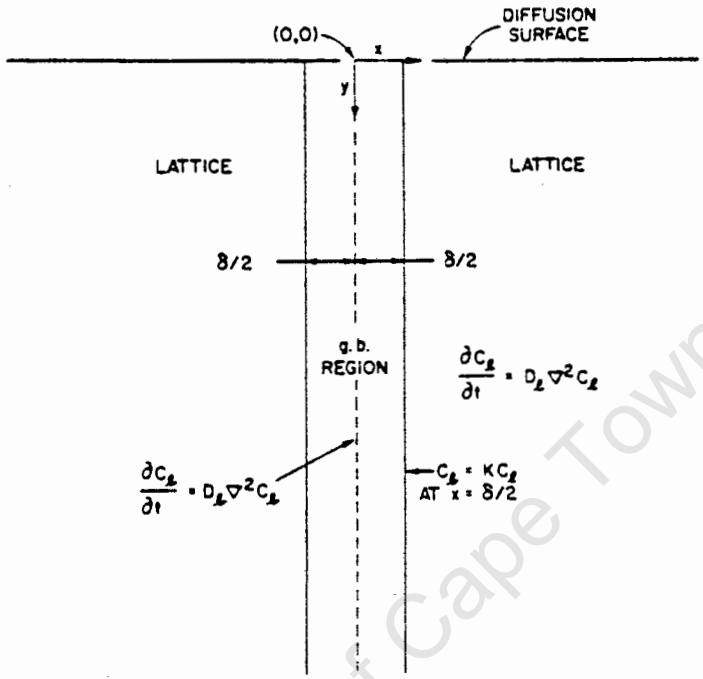


Fig. 1.7 The geometry of the Whipple model for a semi-infinite region with parallel grain-boundaries extending from the diffusion surface.



microprobe studies have revealed that the concentration profiles for the thin source case are significantly different from those predicted by the Whipple model. Suzuoka [ 54 ] has modelled this situation assuming an instantaneous source condition, and has been able to reproduce the observed concentration profiles. Gilmer and Farrel [ 55 ] have obtained analytic and numerical solutions to the grain boundary problem for the case where the

sample is finite in extent. They have shown that the grain boundary diffusion in thin films is very different from the semi-infinite case. They have extended their model to take into account multiple grain boundaries, as well as a variety of back surface conditions such as rapid surface diffusion and chemical removal of the diffusing species from the back surface [ 56 ]. Unnam et al [ 57 ] have numerically modelled grain boundary diffusion for the non-linear case. They illustrate the usefulness of numerical techniques as opposed to analytical solutions which are generally exceptionally cumbersome and unwieldy and which in themselves often need numerical integration to obtain final results.



### 3.4. Diffusion controlled growth

Early work on diffusion limited growth was investigated by Zener [ 58 ] who obtained the basic parabolic time dependence relation. Subsequently, much work on the theory of diffusion controlled growth has been reported for binary diffusion couples [ 59, 60 ]. Gilmer and Farrel [ 61 ] have investigated compound formation when grain boundary diffusion is a possible mechanism of transport. Their results indicate that the presence of grain boundaries can result in a growth rate where the time dependence is not parabolic but proportional to $t^r$, where $r < 0.5$ . It has been reported that diffusion controlled growth in thin films may be significantly different from bulk growth processes which are limited by diffusion [ 62 ].

# CHAPTER TWO

# EXPERIMENTAL

## Introduction

The experimental techniques utilised can, broadly speaking, be divided into five categories viz.,

(1) sample preparation and deposition

(2) thermal annealing

(3) rf sputter microsectioning

(4) Beta counting

(5) Rutherford backscattering



## 2.1 Sample preparation and deposition

Single crystal silicon wafers, being readily available, were a convenient substrate to use. Consequently most of the work was carried out using Si<100> wafers ( 1.2-2.8 $\Omega cm^{-1}$ resistivity, n-type ).

### 2.1.1 Sample preparation

Silicon wafers were scribed and washed ultrasonically in a succession of solvents and etchants. The size of the substrate chips was 9mm x 9mm. To degrease the samples and remove unwanted hydrocarbons, the scribed silicon was washed with

trichlorethylene, acetone and methanol. After this sequence of washes, followed by a rinse of deionised water ( resistivity 5MΩ $cm^{-1}$ ), the samples were etched for 5 minutes in a 20% solution of hydrofluoric acid to remove the native oxide layer. Following the technique of e.g. Lau et al [ 1 ], the samples were then washed in RCA solution - ( $H_2O_2$:$NH_4OH$:$H_2O$ in the ratio 1:1:5 ), which causes a uniform layer of oxide to be formed on the surface of the silicon. This layer of oxide was then etched off in 6% HF solution. After diluting the acid solution with deionised water, the samples were lifted out of the solution and mounted for immediate installation in the evaporator.

### 2.1.2 Evaporation

The evaporation system was evacuated by a series of 4 pumps. Firstly, a mechanical forepump was employed to decrease the pressure in the evaporation chamber from atmospheric pressure down to a pressure of about 1 torr. The forepump was isolated from the evaporator by means of a liquid nitrogen cooled cold trap to limit back diffusion of hydrocarbons, i.e. oil from the forepump, into the system. Another precaution to keep the system clean was never to use the mechanical forepump to pump to pressures lower than 1 torr, since use of a forepump to lower pressure is known to result in backstreaming of oil vapour into the chamber being evacuated . Two molecular adsorption pumps, prechilled to liquid nitrogen temperature, were used to further evacuate the deposition chamber down to a

pressure of ~1 X $10^{-4}$ torr. Pumping was continued using an ion pump in conjunction with a titanium sublimation pump. The latter was cycled to fire for 1 minute at 10 minute intervals. Once the pressure was below 1 x $10^{-6}$ torr, a liquid nitrogen cooled cryopanel was used to reduce the pressure further to better than 2 x $10^{-7}$ torr. Prior to, and especially during extended depositions, Ti was evaporated into the system to maintain the integrity of the vacuum.

To deposit metals and silicon a focussed electron beam at 4keV with maximum current capability of 750 mA was directed magnetically onto the material to be evaporated. The materials to be evaporated were seated in copper crucibles which were water cooled. Evaporation rates were typically in the region of 5Å/sec. During evaporation the pressure within the evaporator rose to approximately 5 X $10^{-7}$ torr.

Two configurations were used for sample deposition. In the first, six sample holders mounted on a carousel arrangement allowed for six independent depositions. Each sample holder could accommodate up to 10 samples. In the second configuration, a scribed but uncleaved substrate of 20 samples was mounted on an in situ resistive heating element. This allowed for annealing to be performed inside the evaporation chamber without breaking vacuum. At the end of each complete evaporation high purity nitrogen was introduced into the system until atmospheric pressure was regained inside the chamber.

## 2.2 Thermal annealing

Thermal annealing was carried out either in the evaporation chamber itself or in a separate Lindberg oven, the latter controlled by a Eurotherm temperature controller. The oven allowed up to 40 samples to be annealed per pumpdown by employing a carousel accommodating up to eight quartz boats, each of which could hold a maximum of 5 samples. The pressure in the furnace was always lower than $10^{-6}$ torr and the temperature was allegedly controlled to within 0.5% of the desired value.

In situ anneals were carried out on a resistive in situ substrate heater. This consisted of a flat cylindrical aluminium holder ( not unlike the holders used for normal deposition ) inside which was a pair of resistive heaters. The temperature was controlled by a Type K thermocouple and digital temperature controller. Throughout anneals the temperature was recorded. In general, the temperature of the substrate rose at a rate proportional to time during heatup, and during the quenching stage, heat was lost at an exponential rate. When it was necessary to cool the heating element at the end of an anneal, an aluminium block of approximately 5 times the heat capacity of the substrate heater was lowered onto the substrate heater.

## 2.3 R F sputtering

Microsectioning of prepared samples ( for depth profiling ) was carried out using r.f. sputtering. A stable r.f. signal generator capable of delivering 400 watt was used to generate an $Ar^+$ plasma at a frequency of 12.33MHz. The samples to be sputtered were fixed to the cathode of the appliance with silver paste. The cathode was water cooled and since good thermal connection was ensured by the use of the conductive silver paste, it was believed that during sputtering, the temperature of the sample was lower than 100°C. Spectrographic argon was supplied to the sputtering chamber via a needle valve and the pressure was maintained at $6.0\pm0.5 \times 10^{-3}$ torr throughout the sputtering. A forward power of 100 watt was used to sputter the samples.

## 2.4 Rutherford backscattering spectrometry

Rutherford backscattering is a well established technique which is useful for surface and thin film analysis. The technique derives its usefulness from three basic concepts, viz.

(i) the energy loss of bombarding particles upon elastic scattering

(ii) differential scattering of particles depending on the nature of the target

(iii) energy loss upon traversing a layer due to loss of energy to the target atoms.

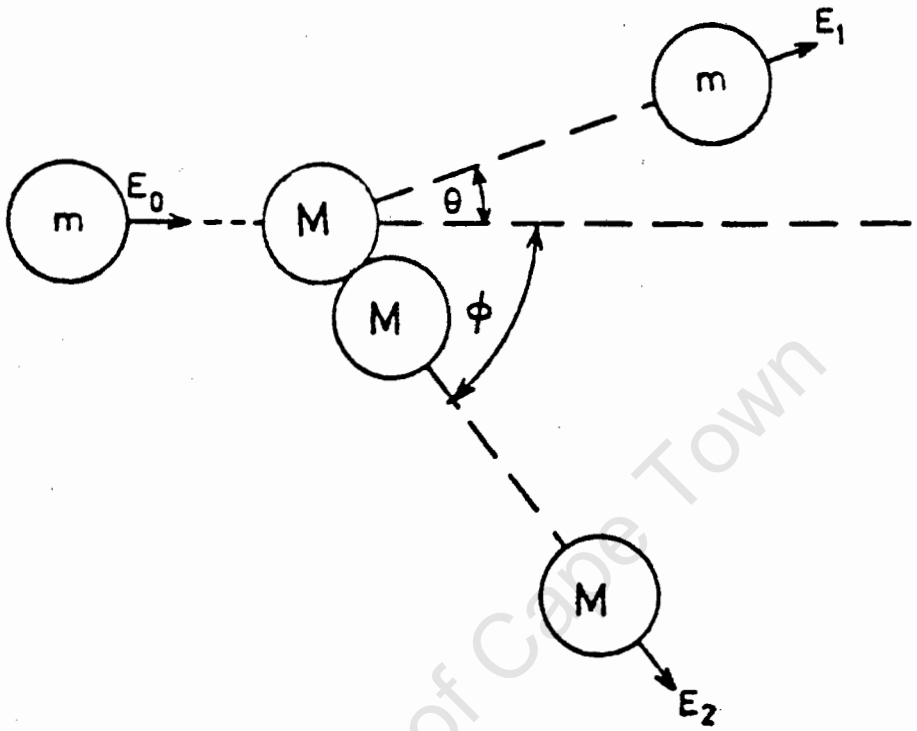


Fig. 2.1 Schematic of an α-particle undergoing an elastic collision.



We now discuss the three concepts more fully and develop a practical means of utilizing them to extract useful information about thin film metal silicides.

(i) A projectile of mass, m, and energy, $E_o$, colliding with a stationary target particle of mass, M, undergoes a momentum transfer and in the process loses kinetic energy in accordance with the relation

$$E_r = \frac{E_o\,(m\cos\theta + [M - m\sin^2\theta]^{\frac{1}{2}})^2}{m + M} \qquad [\ 2.1\ ]$$

$$= KE_o$$

where θ, the scattering angle, is measured in the laboratory frame of reference. $E_r$ is the recoil energy of the scattered particle and K is the "kinematic factor". Therefore, knowing the incident and the recoil energy of the projectile along with its mass and scattering angle, one can determine the mass of the scattering target.

(ii) The differential scattering cross section, dσ/dΩ, is given by

$$\frac{d\sigma}{d\Omega} = \left(\frac{Z_1 Z_2 e^2}{2E\sin^2\theta}\right)^2 \frac{\{\cos\theta + [1-(\frac{m}{M}\sin\theta)^2]^{\frac{1}{2}}\}^2}{[1-(\frac{m}{M}\sin\theta)^2]^{1/2}} \qquad [\ 2.2\ ]$$

where θ is the scattering angle in the laboratory frame

m, M are the masses of the projectile and target particles respectively.

E is the energy of the projectile immediately before scattering, and

$Z_1$, $Z_2$ are the atomic numbers of the respective projectile and target particles.

The scattering yield is related to the probability of a scattering event occurring and therefore qualitative measurements concerning the abundance of a scatterer of known mass and density can be made.

(iii) A particle traversing a thin film will, in general, lose energy to the surrounding electrons by excitation and ionisation. The rate of energy loss per unit distance dE/dX, is found to be dependent on the energy of the traversing charged particle. Knowing the rate of energy loss as a function of depth will fix the energy of a projectile at a given depth if the initial energy of the projectile is known. The energy loss parameter, dE/dX, as a function of E and and X, has been determined for all elements and can be well approximated by a fifth order polynomial. Integration of the energy loss with respect to the depth therefore enables computation of the energy of a particle at a given depth if the initial energy is known.



By combining (i) and (iii) it is possible to perform a depth analysis of a thin film of known composition. Supposing that a monoenergetic beam of particles of known energy is directed at a thin film, one can deduce the thickness of the film using the following scheme. A beam of particles directed at a thin film, as illustrated in figure 2.2, will undergo backscattering at various depths in the film. In particular, some particles will be backscattered from the surface of the film while others will undergo scattering at the back of the thin film. A particle of

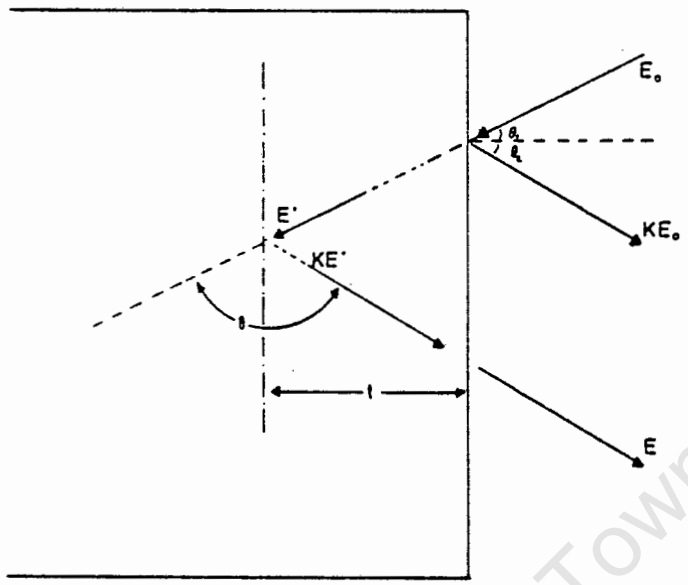


Fig. 2.2 Illustration of an α-particle undergoing Rutherford backscattering after traversing layer of thickness t



incident energy $E_o$, backscattered from the surface of the film, will be detected to have energy $E_1 = KE_o$, as determined by eqn 2.1. Not all particles will be scattered from the surface and those particles which enter the film will lose energy in accordance with the energy loss parameter. A particle which is backscattered from within the film, eg. at some depth, t, will have energy E′, immediately before scattering, where E′ is given by

$$E' = E_o - \int_o^{t/\cos\theta_1} \frac{\partial E}{\partial x}\, dx \qquad [\ 2.3\ ]$$

where $\theta_1$ is the angle which the incoming particle makes relative to the normal to the surface of the sample. The particle will then undergo scattering and the energy immediately after scattering will be $E''=KE'$. The particle then moves toward the surface, losing energy again as it does so and the energy with which the projectile exits the film is given by

$$E = E'' - \int_{o}^{t/\cos\theta_2} \frac{\partial E}{\partial x}\, dx \qquad [\ 2.4\ ]$$

where $\theta_2$ is the angle, relative to the normal, of the outward path. Consequently the difference in energy between a particle scattered from the surface and one scattered from some depth t is given by :

$$KE_o - E = \Delta E = K \int_{o}^{t/\cos\theta_1} \frac{\partial E}{\partial x}\, dx + \int_{o}^{t/\cos\theta_2} \frac{\partial E}{\partial x}\, dx \qquad [\ 2.5\ ]$$

For the case where the film is a compound comprised of two elements, A and B, in the ratio of X:Y, i.e. some compound whose stoichiometry can be described as $A_xB_y$, Bragg's law of linear superposition may be applied with the effects of each scatterer being linearly additive in proportion with their relative atomic abundances. In other words, scattering and energy loss are assumed to occur in proportion to the relative amounts of each type of constituent atom present in the compound. Alternatively

the law of superposition can be viewed as meaning that the physical interactions of one type of atom present in the compound with the bombarding beam are independent of interactions of other constituents with the beam. As an illustration of the superposition principle, let us consider backscattering of a $Pd_2Si$ film. The $Pd_2Si$ lattice has 2 Pd atoms for every 1 Si. Therefore, since $Pd_2Si$ has a density of $2.4 \times 10^{22}$ atoms $cm^{-3}$, the density of Pd atoms in $Pd_2Si$ will be $1.6 \times 10^{22}$ atoms $cm^{-3}$ and of Si, $0.8 \times 10^{22}$ atoms $cm^{-3}$. Consequently, a beam of charged α-particles passing through the film, will lose energy as though 1/3 of the particles were silicon and 2/3 were palladium. To calculate the energy loss of the beam as it traverses some small element of thickness ΔX one needs therefore, to obtain the quantity:

$$\Delta E = \frac{1}{3}\left(\frac{dE}{dX}\right)_{Si}\Delta X + \frac{2}{3}\left(\frac{dE}{dX}\right)_{Pd}\Delta X \qquad [\ 2.6\ ]$$

where the subscripts for the energy loss rates denote the element responsible for that energy loss. Clearly, therefore, the rate at which an α-particle loses energy while passing through a compound crystal depends linearly on the relative amount of each element as well as on the energy loss parameter for that element.

The experimental arrangement employed was to direct a collimated beam of 2 MeV alpha particles ( $He^{2+}$ nuclei ) at a sample which was mounted on a moveable ladder. Up to twenty standard size

samples could be mounted simultaneously on this ladder. By moving the ladder in the vertical direction samples could be moved into the path of the beam. The scattering angle was set at $165^{o}$ in the laboratory frame of reference by adjusting the angle made by the sample relative to the beam. A solid state detector held at a regulated D.C. bias of 50 volt was set at $165^{o}$ to the incident beam. The pulses generated by scattered particles impinging on the solid-state detector, were processed and displayed on a multichannel analyser which provided discrimination of approximately 4keV per channel. Calibration was obtained by measuring the backscattered energy from the surfaces of gold, cobalt, silicon and palladium films. The back-scattering chamber was held at a pressure of $<1 \times 10^{-4}$ torr. Generally, the measured backscattered current was around 150 nA to maintain the dead time at less than 5%. Total integrated currents of $2 \times 10^{-5}$ C were used to ensure reasonable statistics. In the case of certain measurements where low noise requirements were essential, currents of < 50 nA and accumulated charge of $5 \times 10^{-5}$ Coulomb were aquired.



## 2.5 Radioactive tracer techniques

To perform radiotracer measurements, ultrapure silicon was irradiated overnight at the reactor facility of the Atomic Energy Board at Pelindaba. The silicon was placed in a thermal neutron flux of $2.5 \times 10^{13}$ neutrons $cm^{-1}s^{-1}$. A naturally occurring silicon isotope, $^{30}Si$, undergoes neutron capture via the reaction:

$$^{30}Si + n \rightarrow {}^{31}Si + e^- + \nu$$

and in the process yields radioactive $^{31}Si$ which decays via beta decay to $^{31}P$. The natural abundance of $^{30}Si$ is only 2.9% and together with the low neutron capture cross section of 0.1 barn, only a minute fraction of the silicon becomes activated. The radioactive silicon decays with a half-life of 2.62 hour and with a maximum beta energy of 1.48 MeV. Due the short half life of the activated silicon it was necessary to complete radiotracer experiments within 24 hours of removal of the $^{31}Si$ from the reactor. The short half life together with the low concentration of $^{31}Si$ make the use of the material relatively safe. The use of $^{31}Si$ is also favoured since, from a chemical ( i.e. via an electronic interaction ) point of view this isotope is expected to behave in a very similar way to naturally occurring silicon. Since the resulting $^{31}P$ concentration is small, it is believed that its presence does not seriously influence the chemical environment within the silicide. Measurement of the beta emmitted during the decay reaction was carried out using a Geiger-Muller arrangement with a pulse shaper, scaler and counter. The background radiation level was determined during each experiment and was found to be constant over a period of over 1 year.

The technique of radiotracer sectioning was to measure the activity prior to and after sputtering. In this way the relative amount of activity removed could be determined. Beta

counting aquisition duration was 300 seconds and, at worst ( such as at the end of an experimental run when about six half-lives had elapsed since removal of the activated silicon from the reactor ), calculated uncertainties in this measurement were expected to be about 10%. Typically the error in the measurement was around 5%.

# CHAPTER THREE

## DETERMINATION OF DOMINANT MOVING SPECIES

### 3.1 Introduction

Deposited titanium has been used as an inert marker to determine the dominant diffusing species during the growth of poly-crystalline $Pd_2Si$ on Si<100>. DMS determination has also been carried out for a $Pd_2Si$ structure where approximately 300Å amorphous Si has first been deposited onto the Si<100> substrate. To justify the second investigation, we note that for radioactive marker experiments to be unambiguous in their determination of the diffusion mechanism during silicide growth, it is necessary to combine the results with inert marker data. Consequently, we use an inert marker not only to determine the dominant moving species during the growth of $Pd_2Si$ on Si<100> substrate, but also to augment radioactive tracer determinations. Therefore we investigate the DMS for exactly the same structure which we use to determine the mechanism of $^{31}Si$ diffusion in $Pd_2Si$ during the growth of $Pd_2Si$, viz. where 300Å amorphous Si is deposited prior to the Pd layer.

The basic idea was to deposit a small amount, ( ~10 Å), of titanium between the interacting silicon and palladium layers, and then measure the displacement of the marker with ensuing silicide growth. In a similar experiment, Ho et al [ 36 ]

measured the movement of the marker by annealing 1550Å Pd on various Si substrates for several different lengths of time. They then measured the marker displacement as a function of the thickness of the grown $Pd_2Si$ layer. In this experiment three different thicknesses of palladium have been deposited and the marker movement determined after total consumption of the metal by the growth of $Pd_2Si$. Using this method, the task of determining the depth of the deposited marker is somewhat simplified due to presence of only one phase, $Pd_2Si$, above the titanium.

## 3.2 Experimental

The two structures investigated using deposited markers were prepared by e-gun deposition onto cleaned Si<100> at pressure of approximately $4 \times 10^{-7}$ torr. The deposited structures were

Si<100>/Pd(20Å)/Ti(10Å)/Pd(variable thickness), and

Si<100>/Si<a>(300Å)/Pd(20Å)/Ti(10Å)/Pd(variable thickness)

as illustrated in fig 3.1.

A thin layer of ~20Å palladium was deposited onto the silicon prior to evaporation of the ~10 Å titanium layer. The purpose of this was to diminish interfacial dragging of the marker which

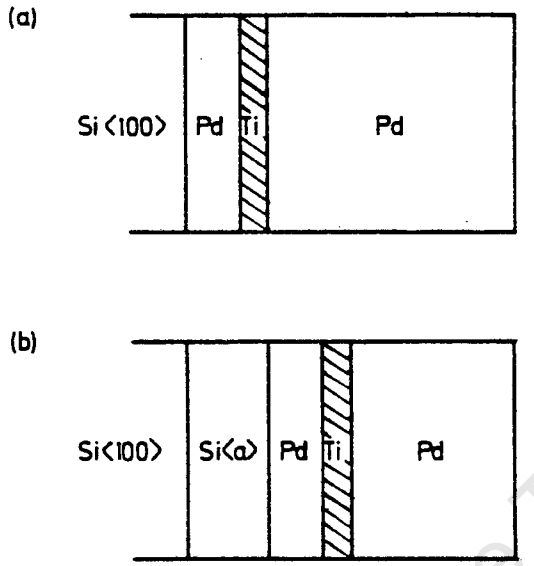


Fig. 3.1 The two structures prepared for determining the dominant moving species during the formation of $Pd_2Si$.



could conceivably be swept along by the advancing growth interface. Three different thicknesses of 600, 1200 and 1800Å palladium were deposited onto the Ti marker layer. After deposition, half of the samples were retained for comparison with the remaining samples which were furnace annealed at temperatures of 250, 300, 350, and 400°C for such time necessary to ensure total transformation of the deposited palladium to $Pd_2Si$. Table 3.1 summarises the various heat treatments to which the samples were subjected. Four different annealing temperatures were chosen because of the likelihood of more than one simultaneous diffusion mechanism - for example, if palladium diffused largely by a grain-boundary mechanism, while silicon

transport was provided by a lattice mechanism, then it could be expected that the relative contribution to the growth which the palladium could facilitate would be largest at low temperatures.

Table 3.1 Summary of thermal annealing of a film with 1200Å palladium deposited.

| Anneal Temp ($^{o}$C) | Annnealing time (minutes) | |
|---|---|---|
| | Si<100> | Si<a> |
| 250 | 71 | 71 |
| 300 | 20 | 20 |
| 350 | 20 | 20 |
| 400 | 10 | 10 |

A Rutherford backscattering depth analysis using 2MeV α-particles was performed for the as deposited and for the thermally annealed samples.



## 3.3 Results

Figure 3.2 presents RBS spectra of two samples before and after thermal annealing at 400$^{o}$C. The thickness of the deposited palladium and the depth of the marker layer was obtained from these spectra. It was found that the position of the Ti marker

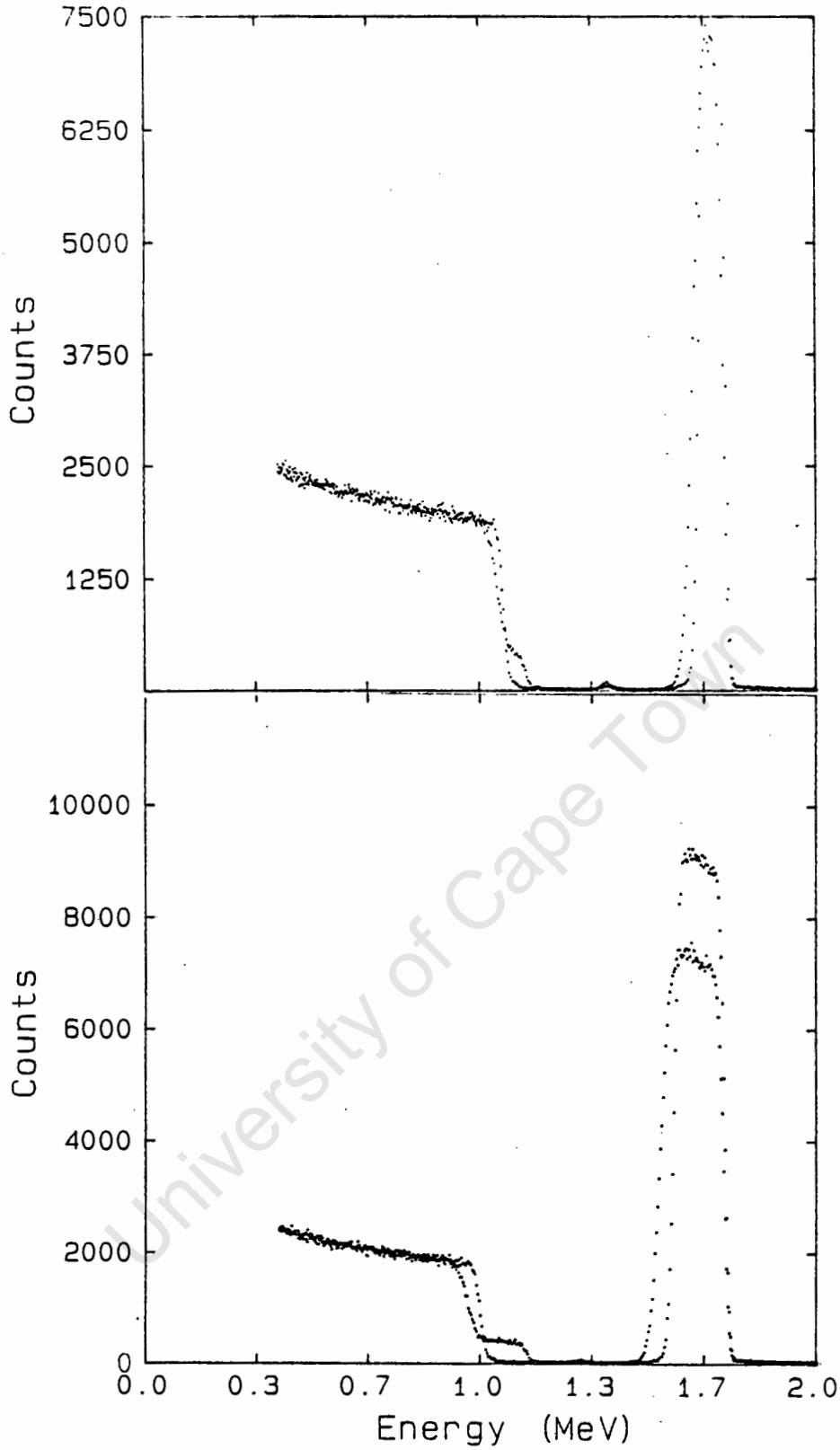




Fig. 3.2 RBS spectra of samples with 800 and 1200 angstrom palladium deposited on Si<100>. Spectra of the samples, which have been annealed at 400°C, are superimposed on spectra of the as-deposited samples.

before silicide formation was consistent with an initial marker location near or at the silicon-palladium interface.

The width of both the Pd and the Si peaks, after thermal annealing, indicates that the amount of silicide formed is in agreement with that expected if complete consumption of Pd had occurred by $Pd_2Si$ formation. It can be seen that there is little difference between the position of the Ti peak for the annealed and unannealed samples. It was noticed that the Ti peak did broaden somewhat after thermal annealing, but the signal remained quite symmetrical. Thus the marker fulfills the marker requirement that spreading should be small and, at worst, symmetrical. The apparent inertia of the titanium peak does not imply that no relative motion of the marker has occurred since the stopping powers of Pd and $Pd_2Si$ are not equal. Analysis of the data, by deducing the amount of Pd or $Pd_2Si$ necessary to shift the titatium peak to the determined position on the spectra, reveals that there is in fact a change in the amount of material on either side of the Ti marker. Table 3.2 summarises data obtained after annealing samples of comparable thickness at various temperatures. In the table the total thickness of silicide grown is given, along with the position of the marker relative to the surface of the sample. A second quantity is also provided viz. the position of the marker relative to the $Pd_2Si/Si$ interface.

It is found that in each of the annealed samples that the Ti marker is positioned in the $Pd_2Si$ approximately 200Å from the $Pd_2Si$/Si interface. In figure 3.3 we plot the deduced marker position (as depth of the marker from the $Pd_2Si$ free surface) as a function of the total amount of silicide grown. It is found that as the total thickness of $Pd_2Si$ increases, so too the marker is buried under an equal amount of silicide once

| 1200Å Pd deposited | ANNEALING TEMPERATURE(°C) 250 | 300 | 350 | 400 |
|---|---|---|---|---|
| SILICIDE | 1620 | 1710 | 1730 | 1660 |
| THICKNESS (Å) | 1650 | 1720 | 1730 | 1680 |
| MARKER | 1470 | 1470 | 1510 | 1510 |
| DEPTH (Å) | 1440 | 1470 | 1510 | 1440 |
| MARKER DIST | 150 | 240 | 220 | 150 |
| FROM Si<100> | 210 | 250 | 220 | 240 |

Table 3.2 Summary of the relative motion of the Ti marker after formation of ~1700Å $Pd_2Si$ at various temperatures. $Pd_2Si$ was grown directly on Si<100>.



~200Å $Pd_2Si$ has been grown. If silicon was diffusing past the Ti marker to form $Pd_2Si$ at the $Pd_2Si$/Pd interface one would expect the depth of the marker to increase at the same rate as

silicide is formed. This type of behaviour is observed after a few hundred angstrom $Pd_2Si$ has formed. It should be pointed out that if only palladium was diffusing, then the Ti marker would always be positioned at or near the $Pd/Pd_2Si$ interface. Plotting this on figure 3.3 would yield a line along the horizontal axis corresponding to a marker depth of zero for all thicknesses of silicide formed. A straight line fit through the data produces a slope which is identical to that which pure silicon diffusion would ensure. Alternatively, one may observe that after an amount of about 200Å of $Pd_2Si$ has formed, that the position of the Ti marker remains quite stable with respect to the $Si/Pd_2Si$ interface. This implies that after an initial amount of about 200Å of $Pd_2Si$ has formed, that palladium transport is negligible. It therefore seems reasonable to assume that once ~200Å of $Pd_2Si$ has formed that Si is the dominant moving species.

From figure 3.3 it can be seen too, that similar results have been found for $Pd_2Si$ grown on the structure which had a 300Å layer of amorphous Si deposited onto the Si<100> substrate. The results of this experiment indicate that the marker motion is consistent with Si contributing some 90% of the total atomic transport during the growth of $Pd_2Si$. Under these conditions, it therefore appears that there is an increased palladium contribution to the transport of material to the growth interface(s).

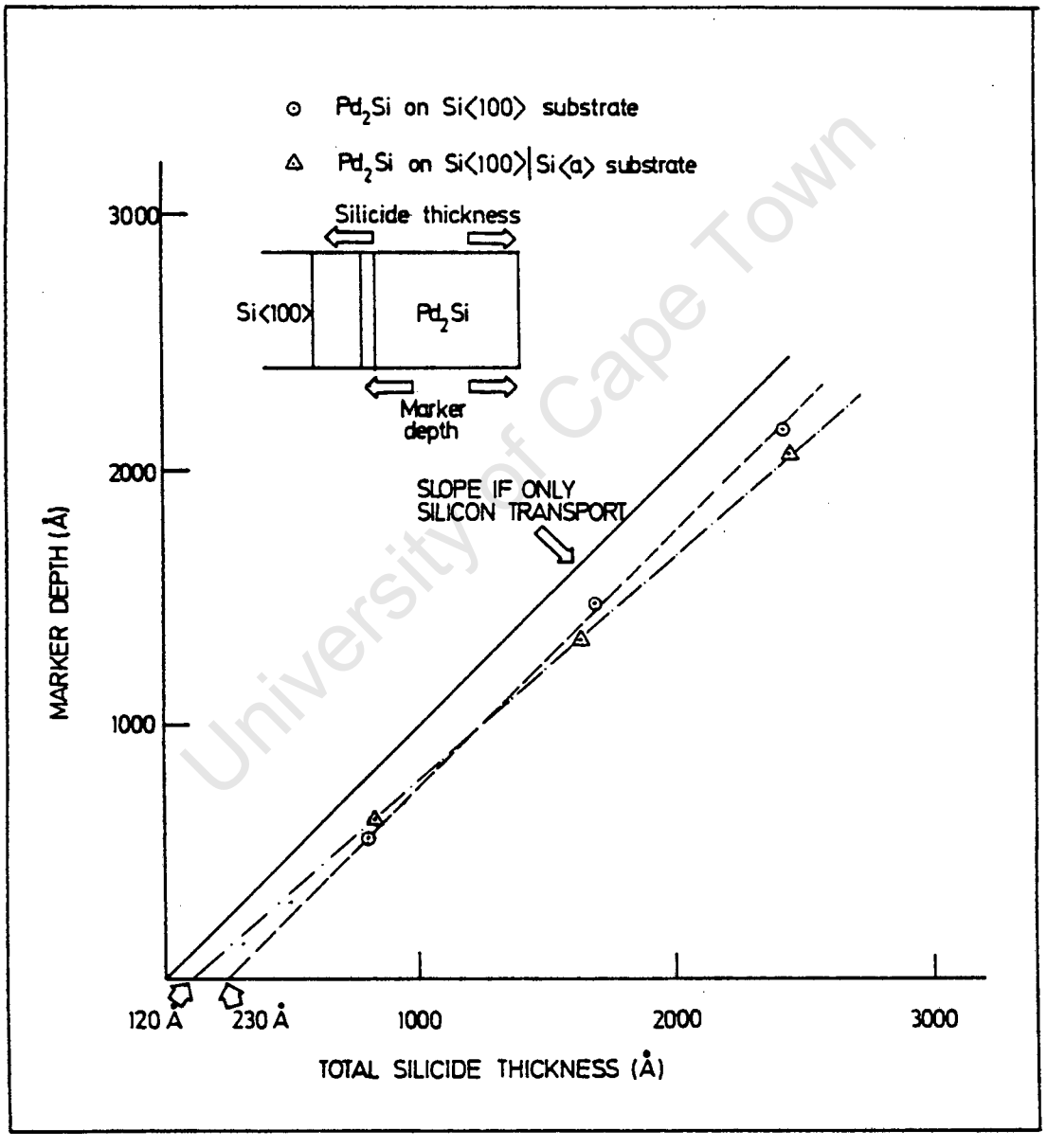




Fig. 3.3 Depth of the titanium marker plotted as a function of the total thickness of silicide grown.

For samples having equal thickness of $Pd_2Si$ it has been found that the final depth of the marker is independent of the annealing temperature over the range 250-400°C. In other words, over this temperature range it has been found that the position of the marker relative to the $Pd_2Si/Si$ interface is more or less constant. While the final placement of the Ti marker layer with respect to the $Pd_2Si/Si$ interface is not exactly the same for all samples, it should be noted that there is no systematic change in this quantity as a function of temperature. The DMS is apparently also independent of annealing temperature in the structure which included the amorphous Si layer.



## 3.4 Discussion

The results of the investigation indicate that the diffusing species during the formation of $Pd_2Si$ is predominantly silicon. The DMS during the initial stages of $Pd_2Si$ is not well established because the the dimensions of the $Pd_2Si$ layer grown was always greater than approximately 800Å. After ~800 angstrom $Pd_2Si$ has formed, however, it appears that silicon transport is solely responsible for the transport of material to the growth interface because the marker depth increases at the same rate as the total amount of grown silicide. It is clear that by the time 800Å $Pd_2Si$ has formed, some Pd motion past the marker has occurred. If only Si movement had occurred during this time, the experimental marker depth should exhibit direct

proportionality with the total thickness of $Pd_2Si$ grown. That the slope of the graph is parallel to, but not collinear with the slope which would result if only Si was the moving species, indicates that some palladium movement has taken place. Since the straight line fit of the experimental marker depth is parallel to the slope indicating only silicon transport (for $Pd_2Si$ thickness >800Å), it is possible to determine the thickness of $Pd_2Si$ which has grown via palladium transport. The offset of the experimental data corresponds to an amount of around 200Å $Pd_2Si$ which has grown with palladium as moving species. That $Pd_2Si$ thicknesses <800Å have not been investigated means that we cannot directly infer when the palladium transport mechanism was operative. However, with regard to the observation that the marker position is independent of the annealing temperature, we argue as follows. The activation energies for Pd and Si diffusion are, in general, not expected to be identical. In particular, if Si and Pd both diffuse simultaneously it would be expected that a variable flux ratio Pd flux/Si flux should be observed when identical samples are annealed at different temperatures. That this is not observed is taken to imply that Pd and Si transport does not occur concurrently. It is interesting to note that Hung et al [ 39 ], using a W marker have observed a marker shift corresponding to 200Å $Pd_2Si$ formed by Pd transport after only 550Å $Pd_2Si$ had formed.

Zingu [ 20 ], has assumed that a stable Si/Pd flux ratio occurs and has calculated this to be 2.0 ±0.6 using a deposited tungsten marker. While the data obtained is in reasonable agreement with the results obtained in this work, the assumption of a constant flux ratio appears to be inappropriate in view of the evidence that both palladium and silicon diffuse but not simultaneously. Hung et al [ 39 ] have performed a tungsten marker experiment to compare the DMS during the growth of $Pd_2Si$ upon thermal annealing and also after ion mixing. They have concluded that both Pd and Si diffuse appreciably with Pd being the faster of the two during thermal annealing. They conclude that Si is the dominant moving species when ion mixing is provided. It is worthwhile noting, however, that after silicide growth had occurred in their experiments, the final position of the W marker was approximately 200Å from the $Pd_2Si$/Si interfaces in both instances. Furthermore, for their thermally annealed samples the total amount of silicide grown was only around 550Å. It is therefore not surprising that they conclude that Pd diffusion is significant during $Pd_2Si$ formation as indeed, during the early stages of $Pd_2Si$ growth it appears that palladium does provide the dominant flux of material for growth. Once the silicide thickness exceeds for example 800Å, however, it appears that palladium transport does not occur to any appreciable degree. The results obtained by the above authors are consistent with the results obtained in the marker experiment described in this work. The results of the Ti marker experiment performed by Ho et al [ 36 ] are in excellent

agreement with our work. The work of Ho et al indicates that the final position of the marker is ~180Å from the $Pd_2Si$/Si interface which is comparable with the value of ~200Å obtained by us.

It has been suggested by Ho et al that, during the initial stages, growth of $Pd_2Si$ is retarded because of the presence of impurities such as the native oxide layer or even the marker itself. They suggest that these impurities inhibit silicon participation in the transport. At this time then, palladium transport becomes activated and presumably continues until the impurities have been adequately incorporated into the silicide layer. Once this has occurred, and silicon transport has been restored, palladium movement is shadowed by the swifter silicon diffusion. In summary therefore, Ho et al propose that the palladium first has to dissolve or incorporate interfacial impurities before a steady flux of silicon can be assured.

The results obtained for the marker experiment performed on an amorphous Si substrate indicate that palladium participation as a moving species persists, albeit to a relatively minor extent, even after a relatively smooth flow of silicon has been established. In light of the view held by Ho et al it can be argued that Pd transport is necessary because the deposited, amorphous silicon can be expected to contain a quantity of oxygen as an artifact of the evaporation procedure. It was in fact often noticed that the samples aquired a brownish colour

just as the silicide formation was completed. This colouration can possibly be an indication of the presence of oxide in the film. If Pd is responsible for dissolving oxides present in the film then this could possibly give rise to a measurable flux of Pd at all stages of growth because this palladium would continually be required to dissolve oxide remnants in the film. However, associated with an increase in the palladium flux, we would expect a decrease in the growth rate. The results of Chu et al [ 32 ], however, indicate that exactly the reverse is true, viz.that the growth rate is largest on Si<a>. This seems to rule out the possibility that Pd transport is activated by the presence of oxide material in the film. It is possible that the enhancement of palladium transport could arise as a consequence of the expected more open environment which would be associated with $Pd_2Si$ grown from amorphous substrate. It would be desirable to repeat this experiment to verify that palladium transport is really enhanced before attempting further explanations of this behaviour.

In summary we conclude that Si is the DMS during the growth of polycrystalline $Pd_2Si$ grown on Si<100> substrate as well as on as substrate which has first had ~300Å Si<a> layer deposited onto the Si<100> substrate. Palladium transport seems to dominate until about 200Å $Pd_2Si$ has formed. Temperature independence of the apparent marker motion during growth suggests that Pd and Si mass transport do not occur concomitantly.

# CHAPTER FOUR

# RADIOACTIVE SILICON TRACER EXPERIMENT

## 4.1 Introduction

Marker experiments using foreign atoms which have been incorporated into the system under investigation use the fact that these atoms are different from those being studied. To establish the relative transport of each species during the formation of a new phase it is a relatively simple operation to measure the quantity of a particular component which has diffused past the marker. One of the major uncertainties regarding the use of marker techniques is the extent to which modification of the transport phenomena occurs in their presence. That marker atoms are not chemically identical with the host is a factor which cannot be overlooked. It is particularly desirable to use other methods to supplement data obtained through the use of these markers.



Since it has been established that silicon is the dominant diffusing species during the growth of $Pd_2Si$ (chapter 3), this knowledge can be exploited to determine the mechanism of diffusion during growth by utilizing $^{31}Si$ as a tracer. Previous work performed by Botha et al [ 47 ], suggests that a substantial amount of mixing of the $^{31}Si$ tracer has occurred after formation of $Pd_2Si$ at 400 $^{o}C$. In their experiment,

For comparison with the abovementioned tracer experiments, another investigation was carried out in which $^{31}Si$ was used as a tracer in a system which included a deposited Ti marker. The reason for this was to check whether a deposited Ti marker modified the diffusion mechanism of silicon during the formation of $Pd_2Si$.

## 4.2 Experimental

### (i) Effect of thickness

Radioactive $^{31}Si$ was deposited onto cleaned Si<100> wafers. After the 300 angstrom deposition of the activated silicon, approximately 1000, 1500 and 2000Å palladium was deposited onto the $^{31}Si$<a> layer (see fig. 4.1 ). The samples were then furnace annealed at 400°C for between 3 and 5 minutes . The length of the anneal was sufficient to ensure complete reaction of the palladium in all three sets of samples. After annnealing the samples, r.f sputter microsectioning was used to determine the distribution of the $^{31}Si$ in the silicide as discussed in chapter 2.

### (ii) Effect of temperature

A structure consisting of Si<100>/Si(a)(300)Å/Pd(2000Å) was prepared by $e^-$ evaporation. This structure was then annealed at

300°C ( for 12 minutes ), 350°C ( 7 minutes ) and at 400°C ( 3.5 minutes ) to completely form ~2800Å $Pd_2Si$ in all three cases. These samples were then sputter profiled and the $^{31}Si$ activity profile determined.

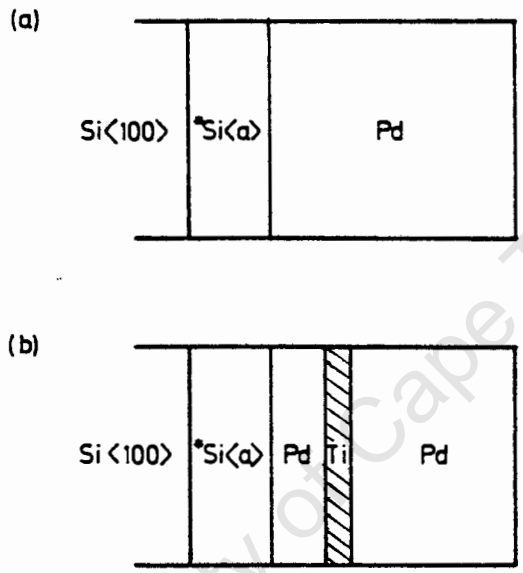


Fig. 4.1 The structures investigated to determine the mechanism of silicon diffusion during the formation of $Pd_2Si$.



(iii) Effect of a deposited Ti marker

The structure, Si(a)(300)Å/Pd(20)Å/Ti(10Å)/Pd(1540Å) was deposited onto cleaned Si<100>. This was subsequently annealed at 400°C for 5 minutes and then sputter profiled.

## 4.3 Results

### (i) Effect of temperature

The RBS spectra for an annealed sample ( 2800Å $Pd_2Si$ ) which has been sputtered for various times is shown in fig. 4.2. The back edge of the Pd peak appears to remain sharp indicating that uniform sputtering has occurred. The thickness of the $Pd_2Si$ layer decreases uniformly with increasing sputter time as is evident from the inset of figure 4.2 in which we plot the amount of silicide removed as a function of time.

The tracer activity profile for a 2800Å $Pd_2Si$ sample which was annealed at 400°C is presented in fig. 4.3(a). In the profile we plot the fraction of activity removed as a function of total amount of silicide removed. Roughly speaking, if silicon diffuses via a vacancy mechanism, then, as detailed in section 1.2.3, most of the activity should lie in a region near the free surface of the sample. If a grain-boundary mechanism was operative, then the activity should be concentrated near to the silicon substrate. The expected tracer profiles are denoted in figure 4.3 by dashed lines. From the figure it can be seen that the fraction of the total activity removed increases at the same rate as the silicide is removed. This clearly does not fit either of the two cases outlined above. The profile can be interpreted more readily if one considers the first derivative

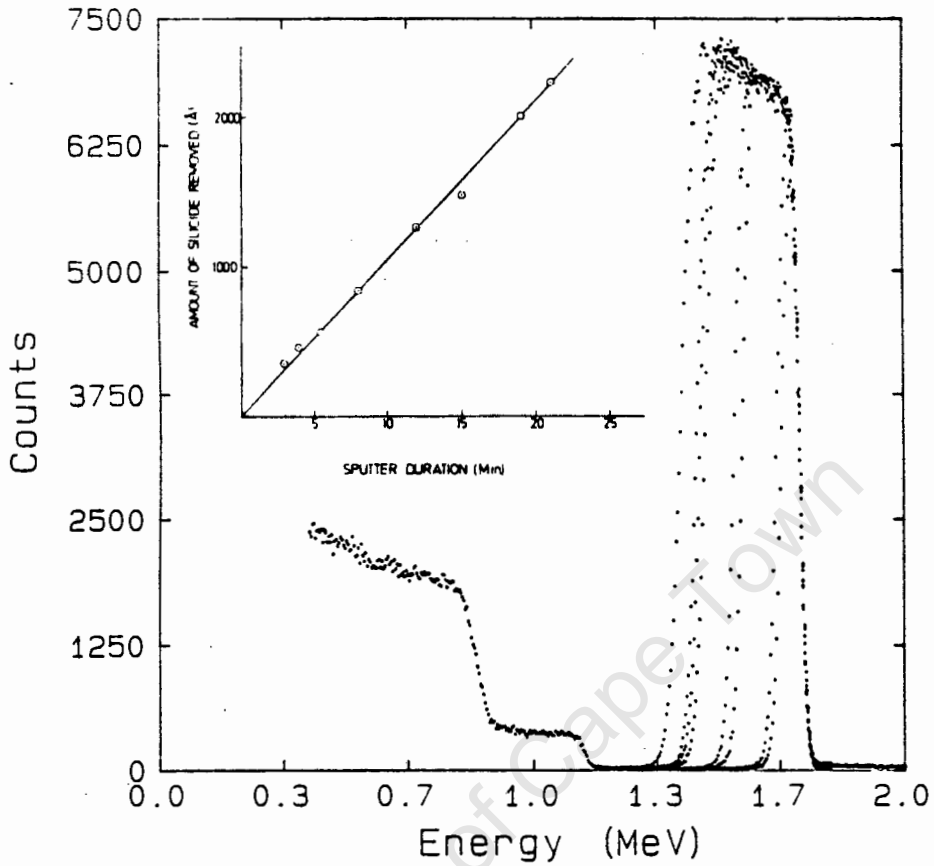


Fig. 4.2 RBS spectra showing the decrease in the amount of $Pd_2Si$ with increased sputtering.
Inset: The amount of $Pd_2Si$ sputtered off is plotted as a function of sputtering duration.



of the experimentally measured profile. Differentiating the profile yields a concentration versus depth profile. Figure 4.3(b) illustrates this and for completeness the expected profiles for grain-boundary and vacancy mechanisms are also included. The experimentally derived concentration profile is flat over the bulk of the sample. This implies that the $^{31}Si$ is distributed relatively uniformly throughout the silicide. At

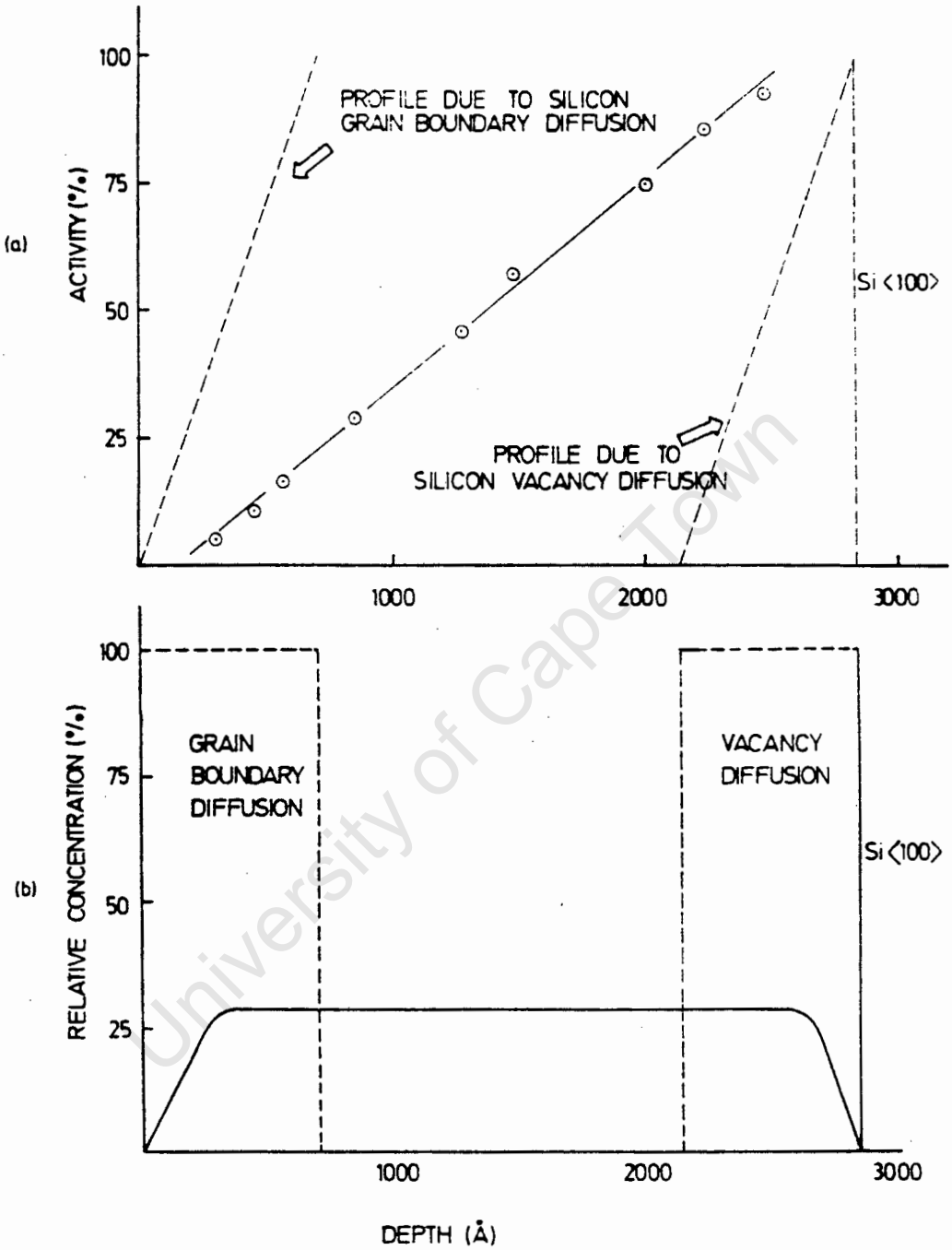


Fig. 4.3 (a) The experimental activity profile for a 2800Å $Pd_2Si$ film after annealing at 400°C for 5 min.

(b) The derived concentration versus depth profile for the sample.

the extremes of the silicide region there appears to be a depletion of radioactive material. In figure 4.4 the activity profiles obtained for each of the three thicknesses of $Pd_2Si$ investigated are presented. The profiles for the three different sized samples are displayed on a common set of axes for comparison. In each case, the data indicates that the amount of $^{31}Si$ removed during sputtering increases in proportion with the total amount of $Pd_2Si$ removed (with the exception of regions close to the free surface and the $Pd_2Si/Si\langle 100\rangle$ interface). This therefore implies that the concentration of $^{31}Si$ is quite uniform throughout a region roughly between 10 and 90% of the $Pd_2Si$ film thickness for each of the three samples.

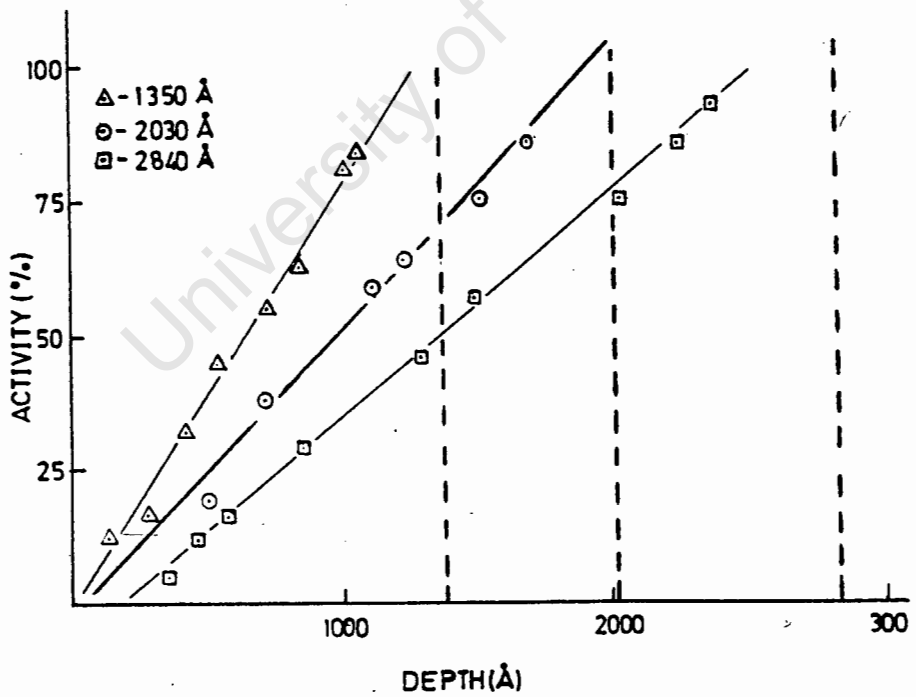


Fig. 4.4 The activity profiles measured for 3 different thicknesses of $Pd_2Si$ annealed at 400°C.

(ii) Effect of temperature

The radioactive $^{31}Si$ profiles obtained after formation of an approximately 2800Å thick $Pd_2Si$ layer at 300, 350 and 400°C are shown in figure 4.5. Since the silicide thickness was not exactly the same for all the samples, we have normalised the data to a constant thickness of 2800Å. It is apparent that the distribution of the $^{31}Si$ is uniform throughout the silicide. With the possible exception of small discrepancies, this feature of uniform distribution of $^{31}Si$ throughout the silicide is independent of the annealing temperature in the range 300-400°C.



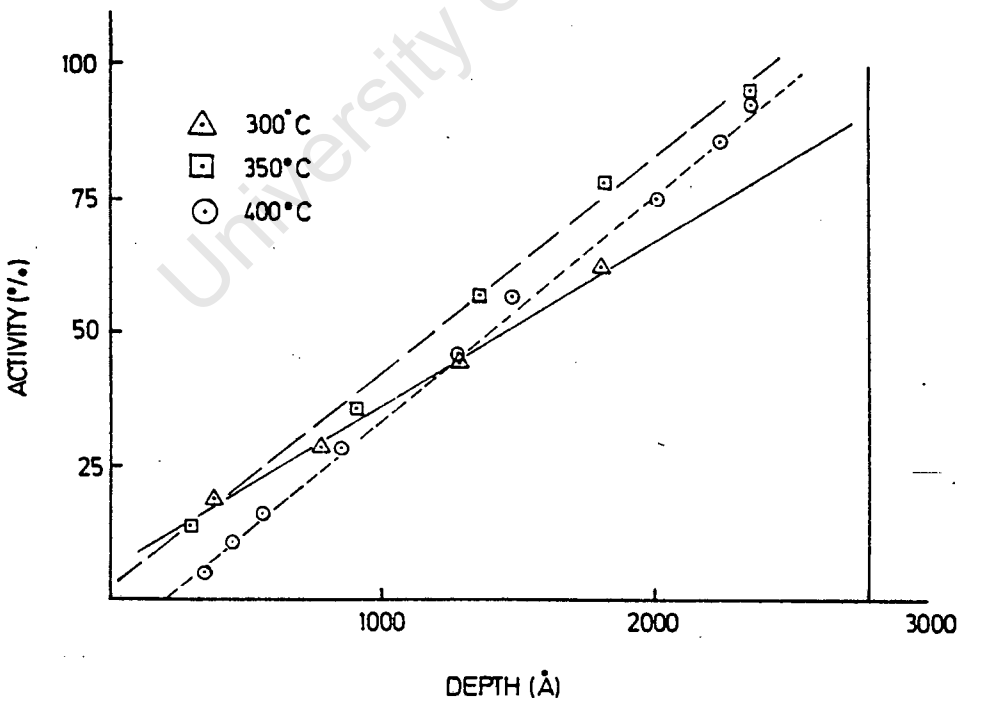


Fig. 4.5 The activity profiles after aneal ing ~2000Å thick samples at 300, 350 and 400°C.

The sample annealed at 300°C appears to be anomalous. The slope of the activity profile appears to be smaller than for the other, higher temperatures. The data seems to suggest that an above average amount of activity is present in a small region near the $Pd_2Si$/Si<100> interface. That this is only observed for the lowest temperature suggests that material may have been locked into this region and can only be liberated by annealing at high temperatutres. It would be desireable to repeat this experiment to determine whether this is a real effect or a chance occurrence.



(iii) Effect of Ti marker

Analysis of the movement of the marker in this sample indicates that after 2150Å $Pd_2Si$ has formed the marker is situated 310Å from the $Pd_2Si$/Si interface. This is consistent with silicon being the DMS. Figure 4.6 illustrates the $^{31}Si$ activity profile obtained after the formation of $Pd_2Si$ with the Ti marker present. Once again the profile obtained appears to suggest a uniformly increasing activity profile as function of amount of silicide sputtered off, implying that in this instance too, the $^{31}Si$ is almost completely intermixed throughout the $Pd_2Si$.

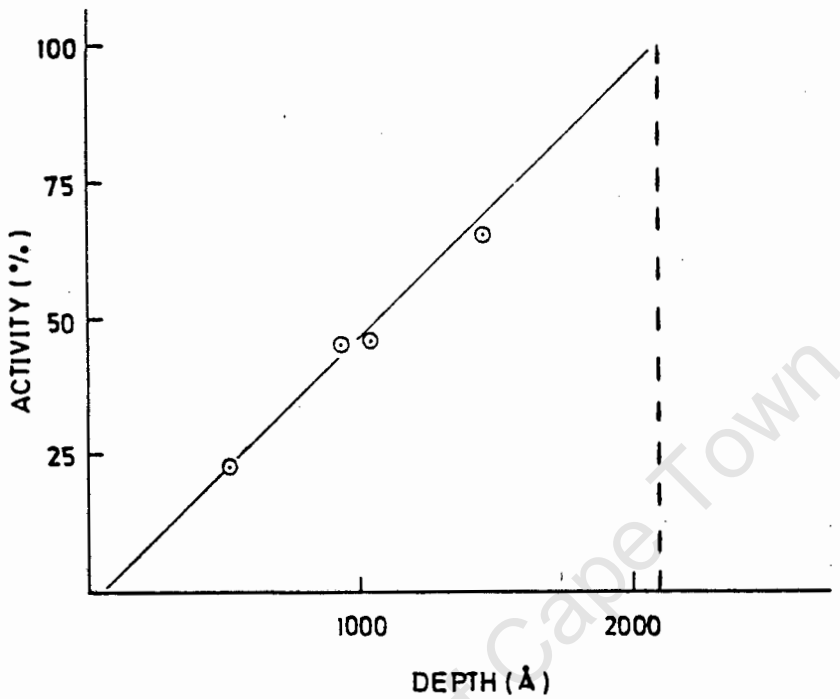


Fig. 4.6 Activity profile obtained with a deposited Ti marker embedded in the 2150Å thick $Pd_2Si$ sample.



All the activity profiles suggest that the $^{31}Si$ has been thoroughly intermixed in the $Pd_2Si$. For completeness we renormalised all the data irrespective of the investigation and present it in figure 4.7 The result is a very convincing straight line which implies that after $Pd_2Si$ formation, the radioactive layer has been intimately mixed with the non-radioactive silicide. From fig. 4.7 one other feature seems to persist viz. the $^{31}Si$ activity increases less rapidly over the last 200Å before the back interface. In terms of a $^{31}Si$ concentration, this implies that the concentration is somewhat reduced near the back interface.

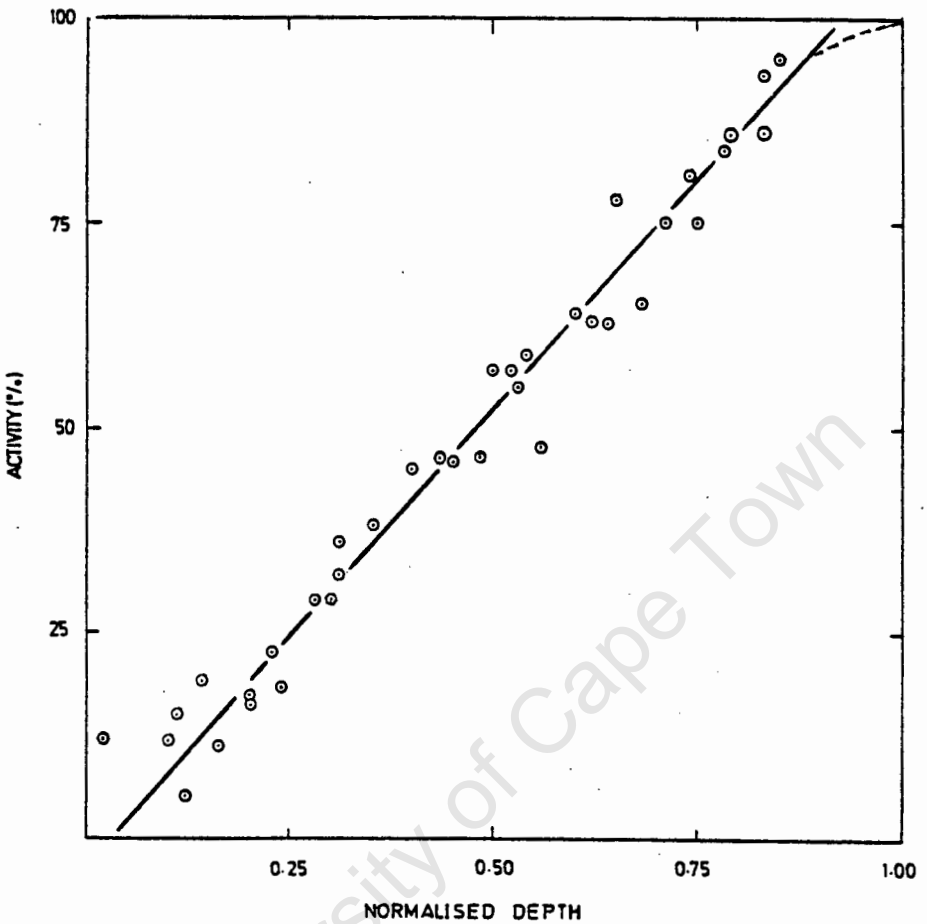


Fig. 4.7 The activity profile obtained by normalising all the data to a common thickness.



## 4.4 Discussion

The flat $^{31}Si$ concentration profile after silicide formation indicates that silicon is highly mobile during or immediately after the formation of $Pd_2Si$. That the profile does not depend on the thickness of the final silicide layer suggests that at all stages of silicide growth the silicon tracer has reached equilibrium with the silicon in the $Pd_2Si$.

The result that the tracer profile is independent of the annealing temperature is strong evidence to support an argument that the diffusion mechanism does not change. Furthermore, since a grain-boundary mechanism would be expected to favour lower temperatures the result that there is no difference in the shape of the tracer profile obtained at 400°C and the lower temperature of 300°C, it would seem unlikely that a grain-boundary mechanism is operative during the growth of the silicide.

The verification that silicon is completely interdiffused even after silicide growth has occurred past a Ti marker lends credibility to the assumption that the Ti should fulfill the requirement of an inert marker, viz. that the transport of material should, be unaffected by the presence of the deposited marker.



It would appear that the spreading of the $^{31}Si$ profile occurs during the growth of $Pd_2Si$. This implies that $^{31}Si$ is highly mobile in $Pd_2Si$ during the growth of the phase. Since the $^{31}Si$ profile is completely spread out, it is not possible to assign a mechanism since it is not known whether the spreading is due to a high self-diffusion of Si in $Pd_2Si$ or whether the growth process in some way enhances the diffusivity of Si. Whether the high mobility is an inherent property of silicon in $Pd_2Si$ or an artifact of the growth process will be investigated in the following chapter.

The cause of the apparent reduction in the activity near the $Si/Pd_2Si$ interface is not clear at this stage. The amount of silicide which is apparently free of $^{31}Si$ is approximately 200Å. This value is reminiscent of the amount of $Pd_2Si$ which ostensibly grows as a result of a flux of palladium. Whether or not there is a connexion between these two measurements is uncertain. If the apparent reduction in activity is real, then it would seem that some mechanism has to be devised whereby silicon transport through this region can occur via some convective mechanism.

# CHAPTER FIVE

## SILICON SELF-DIFFUSION IN $Pd_2Si$

### 5.1 Introduction

The uncertainty regarding the mechanism of diffusion of Si during $Pd_2Si$ formation has prompted an investigation into the nature of silicon self-diffusion in $Pd_2Si$. In the previous chapter it was found that even after ~5 minute anneal at 400°C the $^{31}Si$ tracer was completely flat. This means that complete mixing of $^{31}Si$ with non-radioactive Si had occurred on the Si sublattice during the formation of $Pd_2Si$.

Botha et al. [ 47 ] have measured the self-diffusion of $^{31}Si$ in NiSi and in PtSi. In the case of these silicides, useful diffusion profiles could be obtained even after annealing the silicide at 700°C for 20 minutes. An attempt was also made to measure the self-diffusion of silicon in $Pd_2Si$. However, because the self-diffusion measurements were made after $^{31}Si$ had been used as a radioactive tracer, the "starting profile" was quite spread out (for $Pd_2Si$) before subsequent diffusion anneals could be performed. No self-diffusion measurements were therefore obtained as the starting profile was too spread out to begin with.

It is highly desirable to establish whether the high diffusivity of silicon during the growth of $Pd_2Si$ is a pure thermal effect or whether it arises out of the transport process associated with silicide growth.

The approach which is used in this work to determine the diffusion of silicon in $Pd_2Si$, in the absence of silicide formation, is to grow a structure such that a sharp, well defined radioactive $Pd_2{}^{31}Si$ layer is formed above a polycrystalline non-radioactive $Pd_2Si$ film and then observe subsequent diffusion after thermal annealing of the film.

## 5.2 Experimental

The desired structure was grown after sequentially depositing 1900 Å palladium, followed by 300Å radioactive $^{31}Si$, onto cleaned Si<100> wafers. The samples were then annealed in situ by holding the samples at 300°C for 10 minutes and then quenching. The main purpose of this in situ anneal was eliminate the possibility that $^{31}Si$ could oxidize upon exposure to the atmosphere. The 10 minute anneal usually ensured that all the Pd had just reacted to form $Pd_2Si$. Figure 5.1 illustrates the formation of the desired sample. After the silicide was formed, the samples were installed in the vacuum furnace and annealed at various temperatures in the range 375-550°C for around twenty minutes. After removing the samples from the furnace, the activity in each sample was measured using

a Geiger Counter. After subtracting the background radiation for the counting interval, the total measured activity was normalised to a given epoch. This quantity is termed the normalised initial activity at a standard time. After establishing the activity in the sample

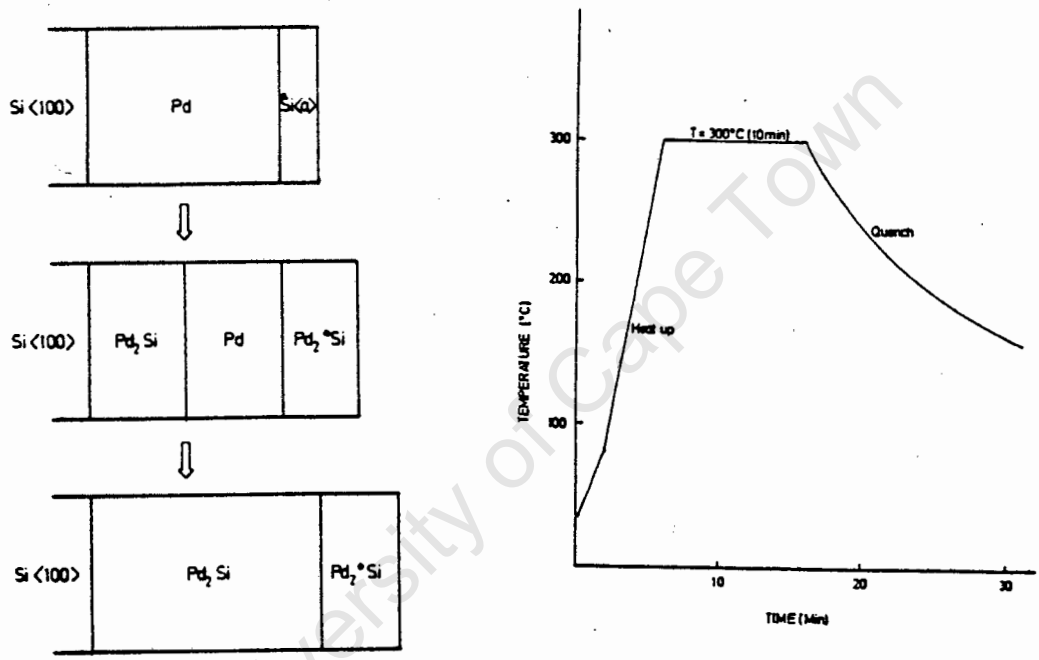


Fig. 5.1 The structure used for the Si self-diffusion investigation. The in situ heating profile is also illustrated.

and determining the uncertainty associated with this measurement, the sample was $Ar^+$ sputtered at 100 watt. The activity remaining in the sample was measured using the same technique as before and the total activity in the removed slice (normalised to the common epoch), determined. The fraction of activity removed was then computed by evaluating the quotient:

activity removed/initial activity. The thickness of the silicide layer was measured after sample sputtering. To obtain the thickness of silicide removed, the thickness of an unsputtered sample was used as reference for each experiment. This method of obtaining the sputter depth in the sample was highly susceptible to systematic error, since any error in the measurement of the solitary standardising thickness would propagate throughout all subsequent thickness determinations. The problem was alleviated to some extent by using the sputter rates as a further calibration check. The sputter rates were found to be fairly uniform with time - an estimated uncertainty of less than 10%. The fraction of activity removed after sputtering was then plotted as a function of silicide thickness sputtered off, to obtain experimental activity profiles.



## 5.3 Results

In situ annealed samples were generally found to have reacted completely. On a few occasions it was noticed that there was a slight depletion of palladium at a position corresponding approximately to the $Pd_2Si/Pd_2{}^{31}Si$ interface. The depletion was thought to arise from small amounts of oxide which had been swept up during the growth of the silicide. The presence of this feature did not appear to lead to any noticeable effect on subsequent analyses. A $^{31}Si$ activity profile for the in situ annealed starting structure is presented in fig. 5.2, along with its derived concentration profile.

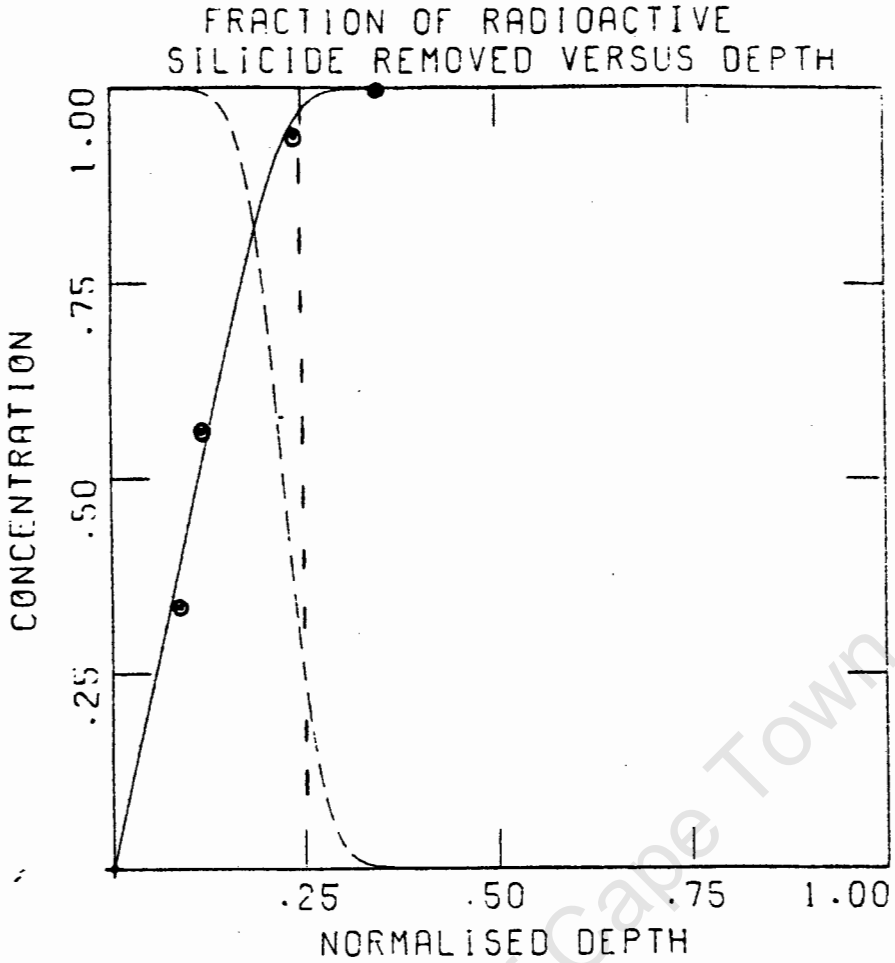


Fig. 5.2 The initial activity (——) and concentration profile (----) for the starting structure.



It can be seen that the $^{31}Si$ is all located in the desired ~600Å thick source region. The requirement that the initial distribution of $Pd_2{}^{31}Si$ should resemble a step function is therefore well satisfied.

RBS spectra of a sequence of sputtered samples are presented in fig. 5.3. A sputter rate calibration curve is presented in the inset. The sputter removal rate is found to be ~230Åmin$^{-1}$ for sputtering of a region which corresponds closely with the $Pd_2Si$ grown from the $^{31}Si\langle a\rangle$ overlayer. Once ~600Å $Pd_2Si$ has been sputter removed, the rate at which material is sputter etched decreases (~130Åmin$^{-1}$) and is also linear with time.

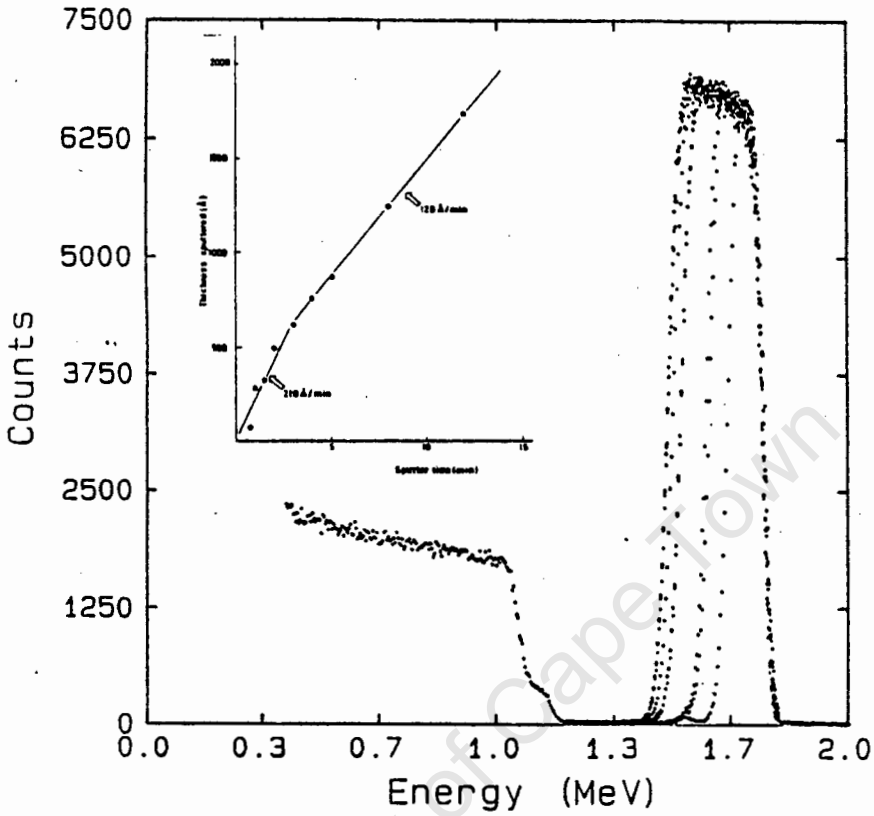


Fig. 5.3 RBS spectra of samples at different sputter times.
Inset: The sputter rate for the utilised structure.



Generally, the sputter rate was least reproducible during the sputter removal of material from the region which had grown on the amorphous $^{31}$Si layer. The reduced reproducibility could be due to contamination at or near the surface of the samples. The faster sputter rate of the near-surface region is thought to possibly derive from the morphology of the amorphous grown silicide.

Using RBS and sputter removal rates in conjunction with β-counting, several $^{31}$Si activity profiles have been obtained.

Figure 5.4 shows the profile obtained after 20 minute annealing of the structure at a temperature of 400°C. Inspection of the activity profile reveals that, during the initial stages of sputtering, $^{31}Si$ is removed at a rate proportional to silicide removal. As more silicide is sputtered off the rate at which $^{31}Si$ is removed drops considerably. At greater depths the $^{31}Si$ is again apparently sputtered off at a rate proportional to the total rate of silicide removal although the rate is considerably lower in this region. Differentiation of the activity profile (with the appropriate renormalisation) yields graph(b) which gives the $^{31}Si$ concentration as a function of depth.



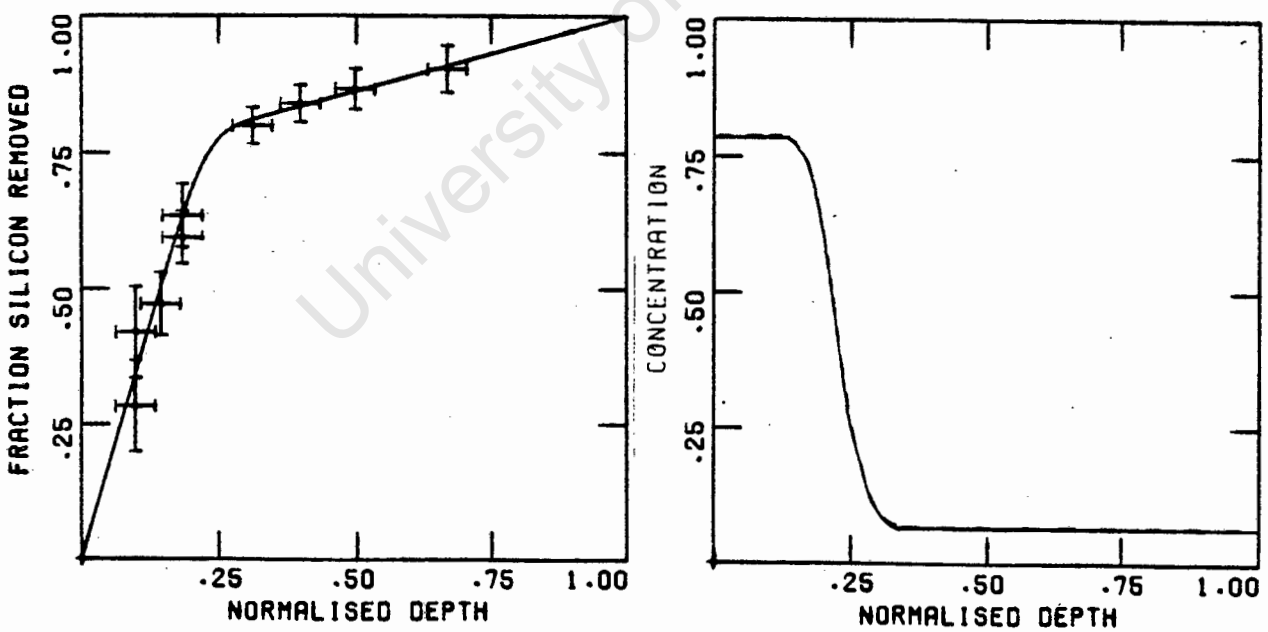


Fig. 5.4 $^{31}Si$ activity and concentration profiles after a 20 minute diffusion anneal at 400°C.

The first and simplest model which was compared with the data was a standard lattice diffusion solution assuming a finite source with reflecting boundary conditions at all edges of the crystal. Figure 5.5 shows various attempts to fit a solution of the above-mentioned model to the data. It can be seen that, at best, reasonable fitting can be achieved only in the region near to the source. It is found that no erf type profile can reproduce the characteristic tail which is prevalent over a large section of the sample.

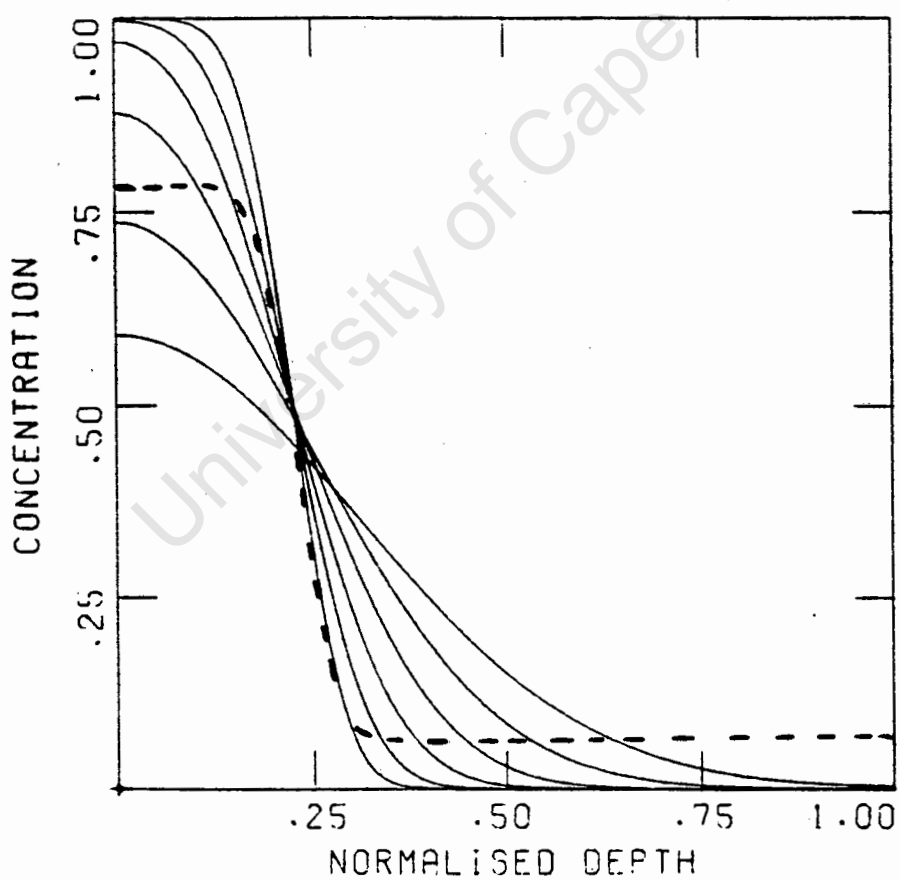


Fig. 5.5 Attempts to fit the experimental profile assuming only lattice diffusion.

The experimental profile which has been found is highly suggestive of a coupled lattice-grain boundary diffusion mechanism [51, 52, 53, 54, 55, 56]. Before pursuing this line, however, we first attempt to show that the anomalous profile is not likely to be an artifact of the experimental procedures which were employed.

Three main possibilities were isolated:

(i) that sputtering of the film was non-uniform and, in particular that preferential sputtering along grain boundaries had occurred. Preferential sputtering would have to be on a sufficiently large scale to be detected by RBS in order to explain the deviation from ordinary lattice diffusional behaviour. RBS spectra did not indicate that preferential sputtering had occurred. Even using SEM to check the lateral uniformity of the sputtered surfaces, it was not possible to observe any such preferential sputtering phenomena.

(ii) A second possibility, that the sputtering process in some way modified the stoichiometry of the silicide, could not be substantiated by RBS.

(iii) A "knock on" effect whereby the sputtering process advanced activated silicon atoms into the silicide would be expected to result in an exponential tail to the concentration profile. The experimentally obtained "tail" was, however,

found to be constant all the way to the rear of the samples. In addition, it was found that as the last of the $Pd_2Si$ was removed so too was the last of the $^{31}Si$. A knock-on effect could have been expected to advance $^{31}Si$ into the Si<100> substrate. It was therefore concluded that a "knock on" effect could not account for the experimentally observed profile.

A model assuming both grain-boundary diffusion and lattice diffusion was adopted ( see appendix A ) . Our model was based on a model due to Gilmer and Farrel [ 55, 56 ]. It was assumed that the structure which was used to study the diffusion could be represented by the geometry shown in fig. 5.6. In our model it is supposed that parallel grain-boundaries run through the entire thickness of the film. Using a grain size of ~600Å and a grain boundary width of ~10Å we are able to qualitatively reproduce the experimentally obtained profiles. A grain size of 600Å chosen represents a typical average ( for 300°C formation of $Pd_2Si$) from numerous literature reports of grain size measurements. The grain size was assumed to be the same for each experiment since, in each case, the silicide was formed at the same temperature viz. 300°C. The grain boundary width of 10Å is merely an order of magnitude estimate. In practice, the grain-boundary width and grain boundary diffusion coefficient can usually not be separated and are presented as a product.

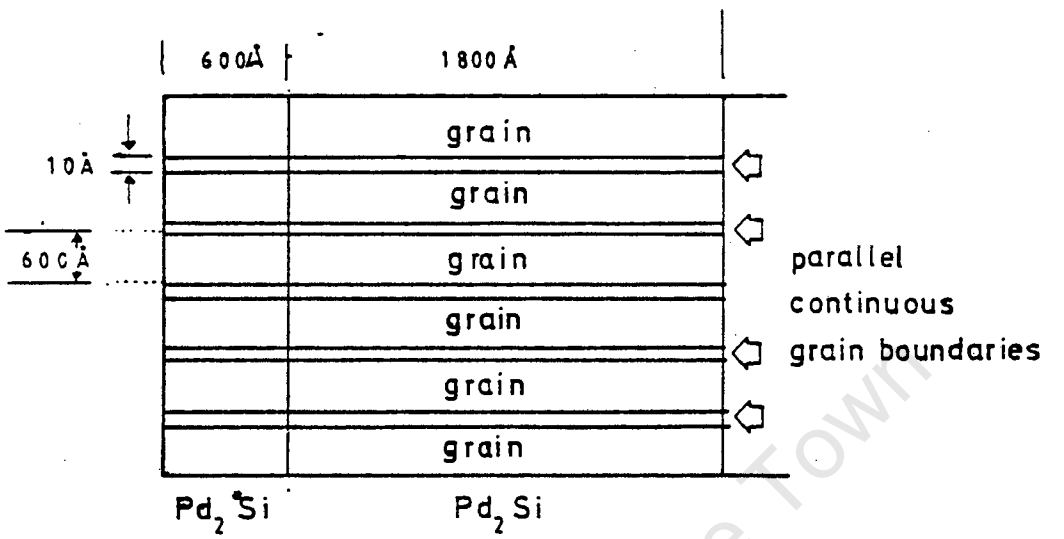


Fig. 5.6 The geometry of the model used to interpret the observed diffusion profiles.

Because the concentration profiles are likely to be less accurate than the raw, experimentally determined profiles, we compare the experimental activity profiles with the integrated form of our solutions to the diffusion problem. Figure 5.7 shows that agreement with experiment is obtained if the model is adopted. The uniform $^{31}Si$ concentration tail which is found to be present right through to the back interface can now be readily explained by the grain-boundary model. It is assumed that the grain-boundary diffusivity is much higher than the lattice diffusion and can therefore easily supply the $Pd_2Si$ with $^{31}Si$ over the entire extent of the silicide . With this assumption the grain boundaries then act effectively as long thin sources for the lattice region. In particular, it is

deduced that the concentration variation as one proceeds down a grain boundary is zero (since the concentration of $^{31}Si$ is constant beyond a depth of ~ 40% of the total film thickness). In other words, the grain-boundaries are effectively saturated and all diffusion in the silicide is limited by the value of the lattice diffusivity.

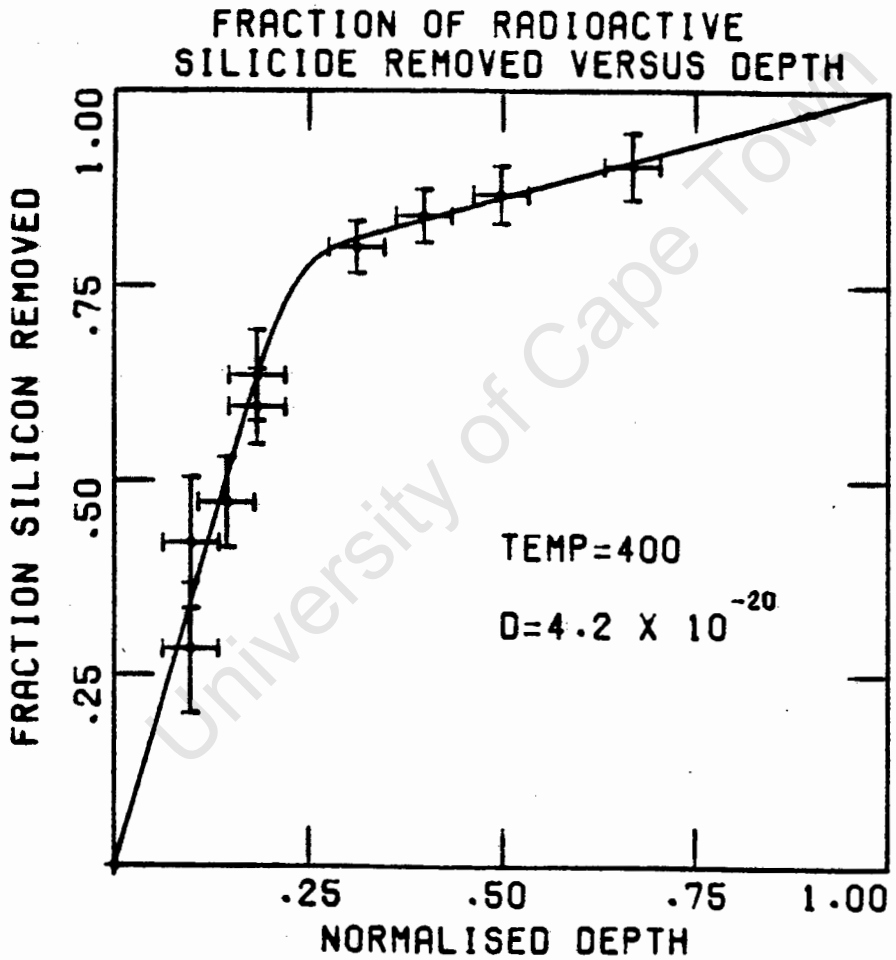


Fig. 5.7 The 400°C experimental activity profile is fitted using the grain-boundary model. The numerical solution assumes a grain-boundary diffusion coefficient of $1 \times 10^{-13}$ $m^2 s^{-1}$ and a lattice diffusivity of $4.2 \times 10^{-20}$ $m^2 s^{-1}$.

The observation that the amount of diffusion was determined only by the particular value of the lattice diffusivity simplified the determination of the diffusion coefficient, since the only free parameter (assuming a fixed grain size) in the model was the lattice diffusion coefficient. Figure 5.8 presents 4 experimental profiles with fitting. The lattice diffusion coefficient was determined for each profile by adjusting this quantity until a best fit to the data was obtained.

It should be stressed that these profiles are obtained under the assumption that an effective grain size of 600Å is representative of the films which were used. Assuming a smaller grain size results in a smaller diffusion coefficient being required to produce the desired profile. Similary, increasing the grain size leads to the requirement that the diffusivity be higher than illustrated in figure 5.8. It was found that the deduced values of the diffusivity differed from those shown in figure 5.8 by a factor of ~2 (greater or smaller) if grain sizes were chosen to be 800Å or 400Å respectively.

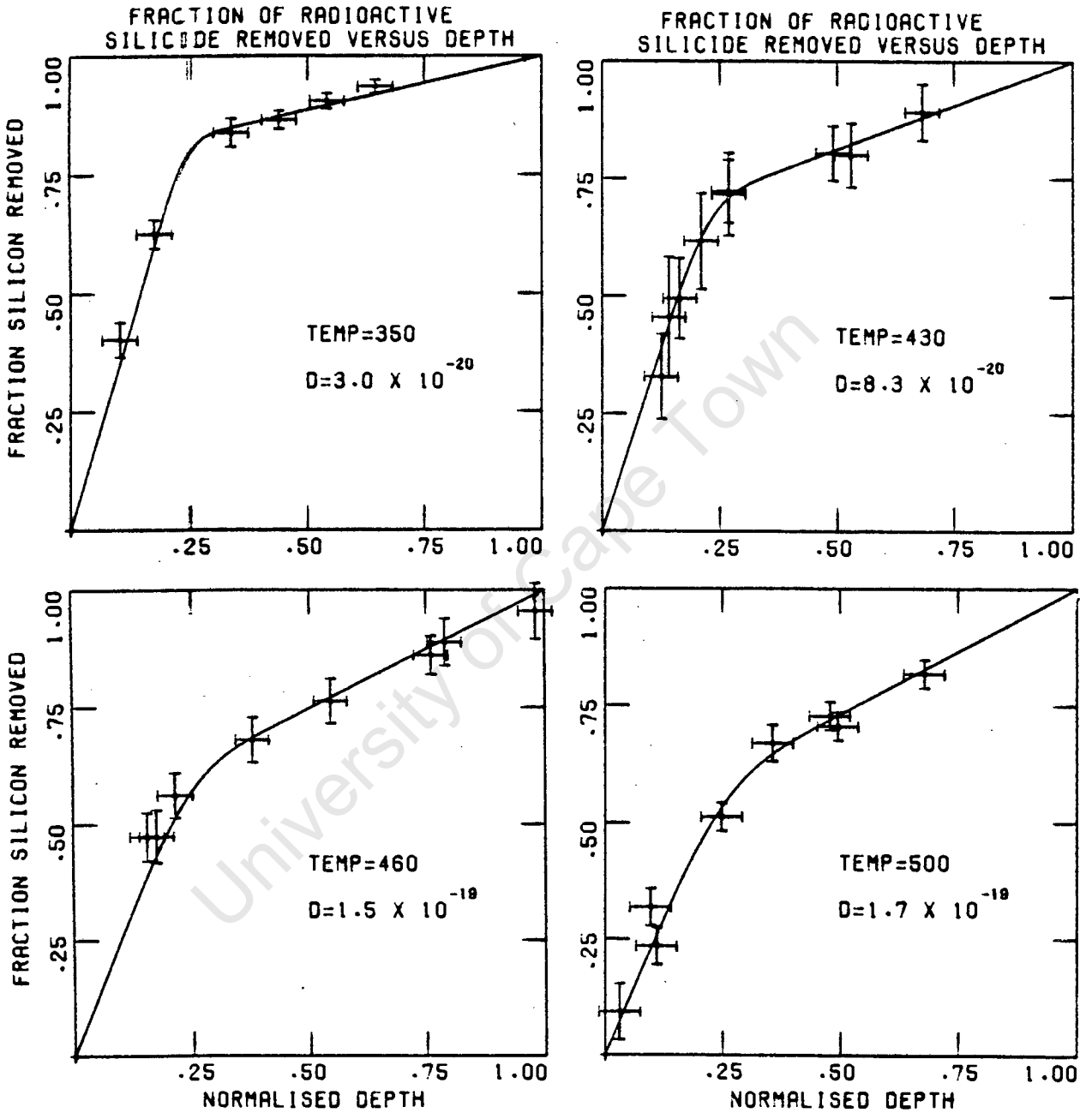




Fig. 5.8 Four experimental activity profiles are fitted. In each case the temperature and the lattice diffusivity are given.

An Arrhenius plot, shown in figure 5.9, is now used to determine an activation energy for the lattice diffusion of Si in $Pd_2Si$. In the plot, the natural logarithm of the deduced diffusivity for each anneal is plotted versus reciprocal temperature. The ln(D) values appear to exibit a linear dependence with reciprocal temperature. It can be seen that there is a considerable amount of scatter in the data. The source of this scatter is not clear, but could result from the presence of uncontrollable amounts of oxide remnants or from uncertainties in the thermal anneal.

The error bars attached to each datum give an indication of the fluctuation of the deduced value of D if the grain size is allowed to vary by 200Å above or below the assumed effective grain size of 600Å. It is possible that the distribution of grain size was not identical for each diffusion anneal. It is interesting that if the grain sizes are consistently scaled up or down, then the slope of the Arrhenius plot does not change appreciably. Assuming that the range of effective grain sizes which have been considered is reasonable, we determine the activation energy associated with (lattice) self-diffusion of silicon in $Pd_2Si$ to be 0.8±0.3 eV. The pre-exponential factor, $D_o$ has been determined to be $4 \times 10^{-(14\pm2)}\ m^2 s^{-1}$.

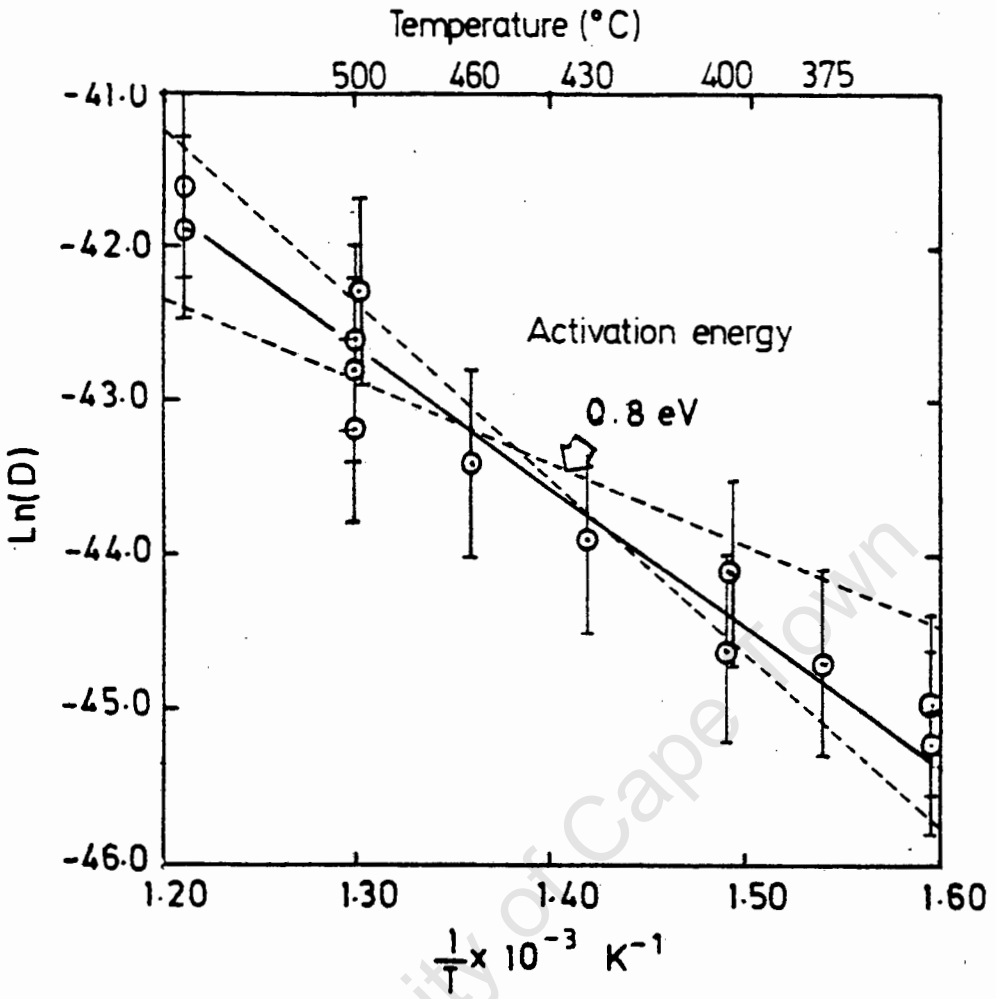


Fig. 5.9 The Arrhenius plot to determine the activation energy of silicon self-diffusion in $Pd_2Si$.



## Discussion

A lattice grain-boundary diffusion model seems to adequately explain the experimentally determined concentration profiles. According to the model, the grain-boundary diffusion is so high that the grain boundaries act as sources because they are in very rapid communication with the entire extent of the silicide. The model provides a qualitative understanding of the mechanism of Si self-diffusion in $Pd_2Si$. The model which has been

developed obviously does not prove that Si diffuses via a grain-boundary mechanism, it merely indicates that a lattice grain-boundary diffusion mechanism is compatible with our experimental results. It is highly desireable that association of a grain boundary mechanism with the observed profiles should be checked by other methods. One suggestion might be that lateral measurements should be attempted to determine whether the $^{31}Si$ (or $^{31}P$ ) concentration is highest in the region of grain boundaries.

The low value of 0.8eV may be unrealistic particularly because of our ignorance concerning the actual grain sizes for each particular diffusion anneal.

After a 20 minute anneal at 400$^{o}$C the $^{31}Si$ tracer profile is far from uniform (see figure 5.8). This means that at 400$^{o}$C, the lattice diffusivity of silicon in $Pd_2Si$ is much lower than when growth occurs at the same temperature. At lower temperatures, for example at 350$^{o}$C, the amount of diffusion which has occurred after a 20 minute anneal is totally insignificant compared with that which occurs during silicide growth at the same temperature. The observed spreading of the $^{31}Si$ profiles can therefore not be ascribed to a high inherent diffusivity of silicon in $Pd_2Si$ .

The results of this work suggest an explanation to the problem of the mechanism of Si transport during the growth of $Pd_2Si$.

If it is assumed that associated with the growth process is a copious production of Si vacancies, then this could cause $D_o$ (which has been determined to be only $\sim 10^{-14}$ $m^2 s^{-1}$) to increase dramatically, and hence facilitate lattice diffusion. In particular, a low activation energy of 0.8 eV could, in conjunction with a sufficiently high value of $D_o$, result in a flat tracer profile after silicide formation.

Finally, we report that tentative investigations indicate that self-diffusion of Si in $Pd_2Si$ which has grown on Si<111> at 300°C, also occurs via a lattice grain-boundary mechanism during thermal annealing in the range 400-500°C. The findings are at present only qualitative. The epitaxial quality of the silicide has also not been ascertained at this stage.

# CHAPTER 6

## Conclusion

It has been found in chapter 3 that silicon is the DMS during the formation of polycrystalline $Pd_2Si$ irrespective of whether it is grown on Si<100> or Si<a> substrate. This result is in agreement with the data of numerous other workers [ 20, 36, 37, 39 ]. The results of chapter 4 indicate that during the growth of $Pd_2Si$, Si mobility is extraordinarily high. The high mobility of silicon during growth is additional evidence that silicon is the dominant moving species. This seems to be borne out by the following empirical observations. Metal is believed to be the DMS during the formation of $Ni_2Si$, PtSi and NiSi. The $^{31}Si$ activity profiles which have been measured after formation of these silicides clearly indicate that the $^{31}Si$ profile is still quite sharp i.e. a significant amount of spreading of $^{31}Si$ has not occurred. In the case of $CrSi_2$, $TiSi_2$ and $ZrSi_2$ the $^{31}Si$ tracer profile is found to be completely spread out after silicide growth. Silicon is the DMS when these silicides form. Baglin et al. [ 65 ], using a radioactive Ni tracer to determine the DMS, find the $^{*}Ni$ tracer is appreciably intermixed after thermal growth of NiSi. In this instance metal is the dominant moving species. It appears, therefore, that associated with the transport of a species to the growth interface, there is an enhancement of the

diffusivity of that species in the new phase through which transport is occurring. That the $^{31}Si$ tracer profile is flat after formation is therefore seen to be supportive of the view that Si is the DMS during the formation of $Pd_2Si$.

In chapter 5 it was found that the self-diffusion of silicon in $Pd_2Si$ is insufficient to account for the marked tracer dispersion which occurs during growth. It has been found that the amount of silicon self-diffusion which occurs in $Pd_2Si$ during a 20 minute anneal at 350°C is orders of magnitude too low to account for the intermixing of $^{31}Si$ which occurs during formation of $Pd_2Si$ at the same temperature.

The activation energy of Si self-diffusion on the $Pd_2Si$ lattice has been determined to be 0.8±.1 eV and the pre-exponential factor $D_o \sim 4 \times 10^{-14}$ $m^2 s^{-1}$. The value of $D_o = 4 \times 10^{-14}$ is low compared with the values obtained by Botha for NiSi ( $D_o = 9 \times 10^{-9}$ ) and for PtSi ( $D_o = 4 \times 10^{-5}$ ). The activation energy for silicon diffusion is apparently very low but this is offset by the low value of $D_o$. The mechanism of silicon diffusion is expected to be a simple mechanism since the activation energy is so low. An interstitial or a vacancy mechanism are therefore seen to be the only likely candidates for the diffusion mechanism. In view of the fact that $Pd_2Si$ has a close packed structure, an interstitial mechanism is probably less favourable than a vacancy mechanism. That the self-diffusion of Si cannot account for the spreading of the silicon tracer profile suggests

that the enhanced diffusivity of the silicon in $Pd_2Si$ is an artifact of the growth process.

During the growth of $Pd_2Si$ it is thought that silicon atoms at the $Pd_2Si$/Pd interface leave the silicide to bond with unreacted palladium at the interface [ 20 ]. The removal of a silicon atom from a lattice site leaves behind a silicon vacancy which is then free to diffuse in the $Pd_2Si$. The silicon vacancy would eventually migrate to the Si/$Pd_2Si$ interface where it would be annihilated by the addition of a Si atom from the silicon substrate. A vacancy concentration gradient could consequently be expected to develop across the growing layer. The vacancy concentration gradient should lead to a corresponding atomic concentration gradient which may be perceptible as a stoichiometry variation across the silicide. It should be pointed out, however, that even a variation of only 1% would be expected to result in a huge increase in the vacancy concentration. The existence of a vacancy concentration gradient across the film would mean that, on average, more atoms would be able to jump in the direction of higher vacancy concentration. Put another way, if the atomic concentration in the growing silicide decreased from left to right, then atoms have available more unoccupied sites to the right than to the left - this would give rise to a net drift of atoms to the right. The important aspect of this argument is that, provided the vacancy concentration is not too large, the potentials surrounding each atom should be largely unmodified and

consequently the activation energy of the atomic jump process remain unchanged. In terms of the diffusion coefficient, therefore, it is expected that the activation energy should remain unchanged, while the pre-exponential factor, ( which is proportional to the vacancy concentration at absolute zero ) should increase with the increased numbers of vacancies. Cheung et al. [ 26 ], and recently Coulman [ 67 ], have reported that the activation energy for growth of $Pd_2Si$ to be from 0.9-1.06 eV. This is comparable to the value of 0.8 eV for Si self-diffusion. The value of $\sim 10^{-7}$ $m^2 s^{-1}$ for the pre-exponential factor of the rate constant which has been obtained by Coulman et al., is $10^7$ times larger than our value of $D_o$. Increasing $D_o$ (for self-diffusion) by a factor of $10^7$, which could presumably occur during the growth of $Pd_2Si$, would explain the flat $^{31}Si$ tracer which has been obtained after $Pd_2Si$ growth.

Because of the reasonably close similarity of the activation energy of growth to that of Si self-diffusion, it is concluded that a vacancy mechanism is highly likely during the formation of $Pd_2Si$ via Si transport. The pre-exponential factor of the parabolic rate constant is also sufficiently high to account for the complete intermixing of $^{31}Si$ in $Pd_2Si$ during the formation of $Pd_2Si$.

In light of the above conclusions it is useful to consider other results which have been obtained by various authors. Lien et al [ 38 ], have used epitaxial $Pd_2Si$ as a "structure marker" to

conclude that Pd is the dominant diffusing species through epitaxial $Pd_2Si$ when polycrystalline $Pd_2Si$ is growing. In their experiment, polycrystalline $Pd_2Si$ was grown above epitaxial $Pd_2Si$. It is observed that as the quantity of unreacted Pd at the free surface decreases, so the thickness of the epitaxial layer increases, while the thickness of the $Pd_2Si$ (poly) remains essentially constant. They suggest that if the $Pd_2Si$(epi)/$Pd_2Si$(poly) interface is stable and $Pd_2Si$ (poly) does not re-register as epitaxial $Pd_2Si$, then growth should occur at the Si<111>/$Pd_2Si$(epi) interface. This then implies that Pd transport is operative and that Si transport does not occur through epitaxial $Pd_2Si$. This then suggests that the microstructure of the epitaxial $Pd_2Si$ prevents Si transport. The implication of this result is that during growth of $Pd_2Si$, silicon transport occurs via a grain-boundary mechanism. This is in contradiction to our result that silicon transport occurs via a lattice diffusion mechanism. In addition, it has been found in this work (see chapter 5), that self-diffusion of Si in $Pd_2Si$ which has grown on Si<111> at 300$^{o}$C, is a lattice-grain boundary process. Whether this indicates that grain-boundary diffusion can occur in epitaxial $Pd_2Si$ is not clear as the epitaxial quality of $Pd_2Si$ formed at 300$^{o}$C is not expected to be very high. In any event, at the temperature at which the Lien experiment was conducted, it seems likely that Si grain-boundary diffusion should not be absent. Our view is that, associated with the consumption of the Pd to form $Pd_2Si$ (poly), is a massive flux of vacancies which flush

through the interposed silicide layers enhancing the re-registering of $Pd_2Si$ at the $Pd_2Si$(epi)/$Pd_2Si$(poly) interface. That epitaxial quality is improved with higher temperature formation as well as by high temperature post-annealing, is thought to support the argument that large numbers of vacancies facilitate epitaxy. In addition, ion implantation of the $Pd_2Si$(epi)/$Pd_2Si$(poly) interface has been shown to enhance the re-registering of polycrystalline $Pd_2Si$ on epitaxial $Pd_2Si$ [67]. In this case as well it is believed that large numbers of vacancies are generated which aid the regrowth of $Pd_2Si$ as epitaxial silicide. It would be interesting to check the results of the above experiment by either utilizing a deposited Ti marker at the epitaxial/polycrystalline interface, or by using $^{31}Si$ for the required Si<a> layer.

Using lateral diffusion measurements, Zingu [ 20 ], has determined the activation energy associated with this growth to be 1.1±0.2 eV. A vacancy mechanism has been proposed in view of the apparent independence of the results on grain size. The observations and conclusions are consistent with our results.

Zingu has also determined the activation energy of Si transport through $Pd_2Si$ when $CrSi_2$ is growing on $Pd_2Si$. The activation energy has been found to be 1.7eV for transport through polycrystalline $Pd_2Si$ and 2.2eV for epitaxial $Pd_2Si$. These results are significantly different from our results. Zingu has pointed out, however, that during the formation of $Pd_2Si$,

palladium atoms are believed to be mobile, whereas during the formation of $CrSi_2$ on $Pd_2Si$, no Pd transport is thought to occur. Inert marker experiments tend to indicate, however, that Pd transport only occurs during the initial stages of silicide growth. It is perhaps not possible, therefore, to explain the high values of 1.7ev(polycrystalline) and 2.2eV(epitaxial) obtained for the activation energy energy of Si transport, in terms of the absence of Pd transport. On the other hand, the results of Lien indicate that Si transport appears to be difficult in epitaxial $Pd_2Si$, would support the result that the activation energy of Si transport in $Pd_2Si$(epi) is high.

(c) The interface between the two silicide layers is expected to be discontinuous and this region should have a high concentration of defects since it marks the line along which the silicide films grown from either side meet. Under this assumption it would be equivalent to define the interface as a grain-boundary. This region could also have substantial amounts of oxides present which could, conceivably act as a diffusion barrier. We do not attempt to include either of the above-mentioned possibilities in the model.

(d) The $Pd_2Si/Si\langle 100\rangle$ interface has been reported by Foll et al to have a relatively high concentration of voids. It has not been attempted to include this structure in the model. It has been assumed that this interface is sharp and that there is no exchange of silicon atoms between the silicon substrate and the silicide.

(e) The free surface, as well as all other boundaries are assumed to be totally reflecting surfaces.

Figure A.1(a) and A.1(b) illustrate the real and ideal geometry of the system. From figure A.1(c) which illustrates 3 adjacent grains, further simplifications become apparent. Firstly, the grains are assumed to be periodically spaced at 600 Å intervals. This implies from symmetry considerations, that the centre of the grain and of the boundary can be considered to be symmetry planes and hence that there is no net flux across these planes.

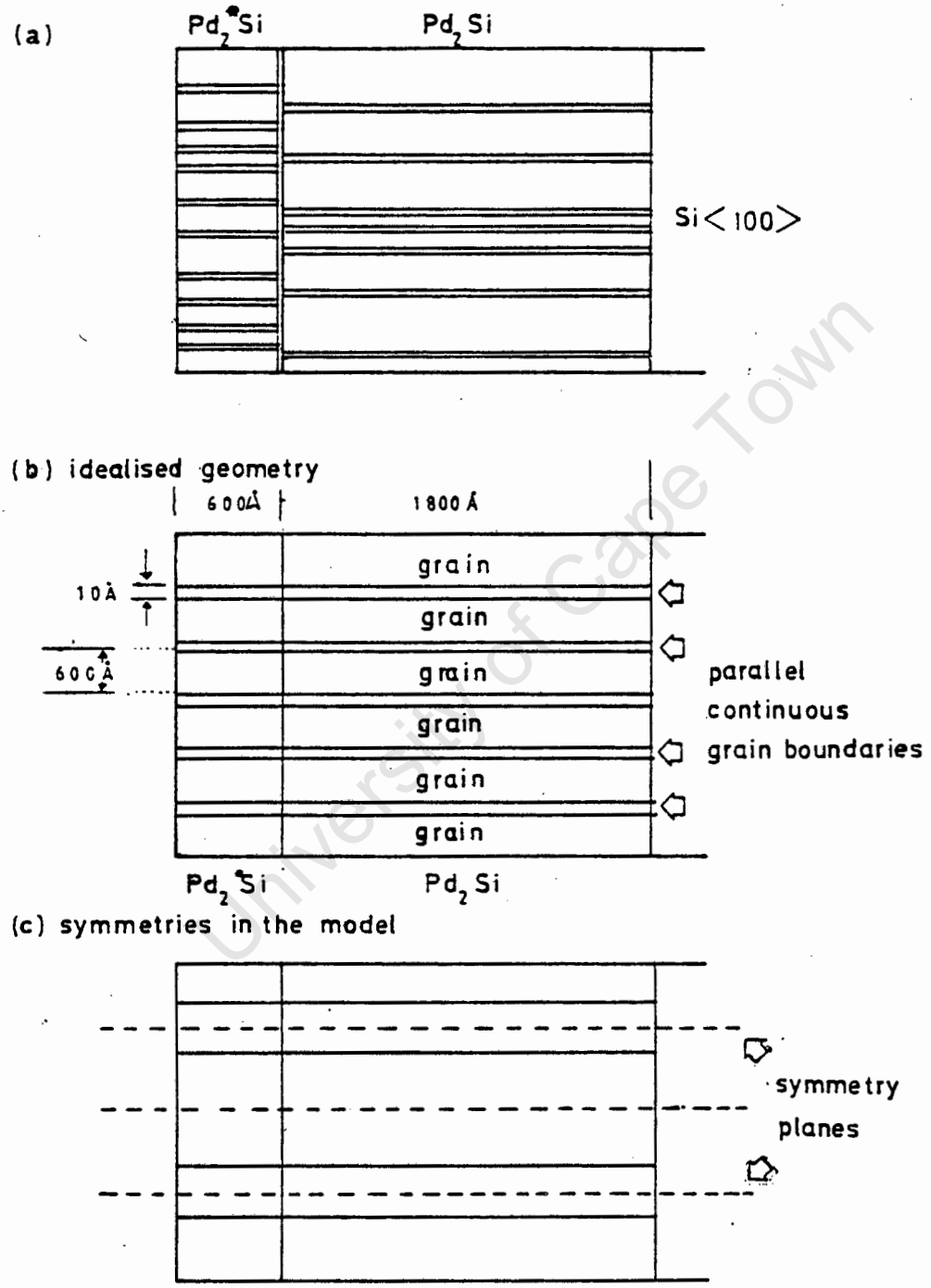




Fig. A.1 (a) The assumed real geometry of the system

(b) The ideal geometry in the model formulation

(c) Symmetries in the geometry of the model

In figure A.2 the following parameters are defined:

$x = L$ is the half-width of the grain

$x = a$ is the half-width of the grain-boundary

$y = S$ is the thickness of the radioactive source layer

$y = Y_o$ is the total silicide thickness

$C_l(x,y,t)$ is the tracer concentration in the lattice

$C_b(x,y,t)$ is the tracer concentration in the grain-boundary

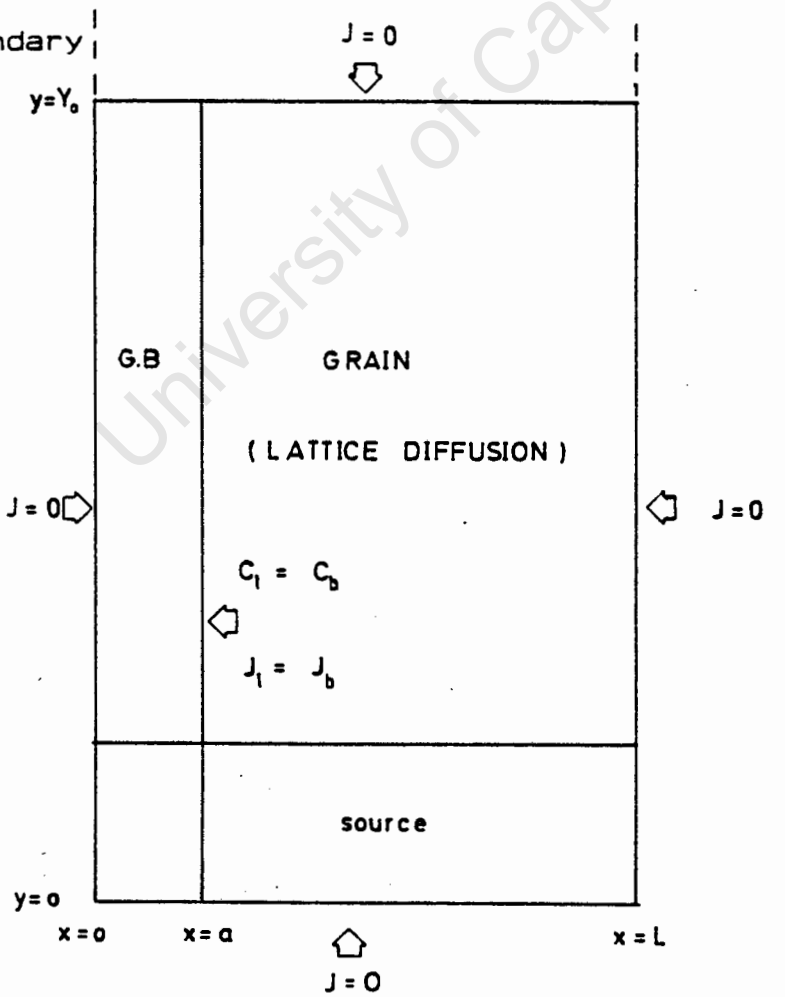


Fig. A.2 The final geometry adopted for the model.

Since x = 0 and x = L are defined to be symmetry planes and as reflecting boundaries give rise to the boundary conditions:

$$\left.\frac{\partial C_b}{\partial x}\right|_{x = 0} = 0 \qquad [\ 1(a)\ ]$$

$$\left.\frac{\partial C_b}{\partial x}\right|_{x = L} = 0 \qquad [\ 1(b)\ ]$$

Similarly, the back interface and the front surface must must also satisfy reflection conditions, viz.:

$$\left.\frac{\partial C_l}{\partial y}\right|_{y = 0} = 0 \qquad a \leqslant x \leqslant L \qquad [\ 2(a)\ ]$$

$$\left.\frac{\partial C_l}{\partial y}\right|_{y = Y_o} = 0 \qquad a \leqslant x \leqslant L \qquad [\ 2(b)\ ]$$

$$\left.\frac{\partial C_b}{\partial y}\right|_{y = 0} = 0 \qquad 0 \leqslant x \leqslant a \qquad [\ 2(c)\ ]$$

$$\left.\frac{\partial C_b}{\partial y}\right|_{y = Y_o} = 0 \qquad 0 \leqslant x \leqslant a \qquad [\ 2(d)\ ]$$

In each region, i.e. the lattice and grain-boundary, the concentration is assumed to satisfy the Fickian diffusion equations :

$$\frac{\partial C_l}{\partial t} = D_{lx}\frac{\partial^2 C_l}{\partial x^2} + D_{ly}\frac{\partial^2 C_l}{\partial y^2} \qquad [\ 3(a)\ ]$$

$$\frac{\partial C_b}{\partial t} = D_{bx}\frac{\partial^2 C_b}{\partial x^2} + D_{by}\frac{\partial^2 C_b}{\partial y^2} \qquad [\ 3(b)\ ]$$

The grain boundary and the lattice are assumed to be in a state of dynamic equilibrium, i.e. that the concentration and flux across x = a both satisfy continuity conditions,

$$C_b = C_l \qquad x = a \qquad [\ 4\ ]$$

$$D_{bx}\frac{\partial C_b}{\partial x} + D_{by}\frac{\partial C_b}{\partial y} = D_{lx}\frac{\partial C_l}{\partial x} + D_{ly}\frac{\partial C_l}{\partial y} \qquad [\ 5\ ]$$

Finally, the concentration variation across a grain boundary is assumed to be adequately approximated by an even, parabolic function such as,

$$C_b(x,y,t) = C_b'(y,t) + x^2 C_b''(y,t) \qquad [\ 6\ ]$$



The problem now is to obtain a solution which satisfies the pair of diffusion equations given by eqns. 3(a) and 3(b) under the boundary conditions given by eqns. 1, 2, 4 and 5. Initially, all the tracer atoms are distributed uniformly in the region $y \leq S$ at time $t = 0$.

The approach which has been adopted is to derive a new set of boundary conditions which hold at x = a and then to solve the lattice diffusion equation neglecting flux inside the grain-

boundary. It is not unreasonable to neglect the flux inside the grain-boundaries, since the grain-boundary width is much less than the grain width, viz. a(10Å) << L(600Å).

The requirement $C_b = C_l$, from eqn 4, implies that for all y along the line x = a

$$\frac{\partial^2 C_l}{\partial y^2} = \frac{\partial^2 C_b}{\partial x^2} \qquad [7]$$

Since $C_l = C_b$ at x = a, this also implies

$$\frac{\partial C_l}{\partial t} = \frac{\partial C_b}{\partial t} \qquad x = a,\ t \geq 0 \qquad [8]$$

$$\frac{\partial C_l}{\partial t} = D_{bx}\frac{\partial^2 C_b}{\partial x^2} + D_{by}\frac{\partial^2 C_l}{\partial y^2} \qquad x=a,\ t \geq 0 \qquad [9]$$

but, using eqn 6, we obtain

$$\frac{\partial^2 C_b}{\partial x^2} = D_{lx}\frac{\partial C_l}{\partial x} \qquad x = a,\ t \geq 0 \qquad [10]$$

$$\frac{\partial C_l}{\partial t} = D_{lx}\frac{\partial^2 C_l}{\partial x^2} + D_{by}\frac{\partial^2 C_l}{\partial y^2} \qquad x=a,\ t \geq 0 \qquad [11]$$

For the purpose of this analysis, it is assumed that $D_{lx} = D_{ly}$ and the lattice diffusion coefficient is simply referred to as $D_l$. Similarly, the grain boundary diffusion coefficient is referred to as $D_b$. The equation which now has to be solved is eqn 3(a) with the boundary condition given by equation 11 and with reflecting boundary conditions along the relevant

boundaries. For convenienience, dimensionless parameters are defined,

$$X = \frac{x}{L} ; \qquad Y = \frac{y}{Y_o} ; \qquad T = \frac{Dt}{Y_o^2} \qquad [\ 12(a, b, c)\ ]$$

$$\alpha = \frac{D_b}{D_i} ; \qquad \beta = \frac{Y_o^2}{L^2} ; \qquad \gamma = \frac{Y_o^2}{aL} \qquad [\ 13(a, b, c)\ ]$$

Equations 3(a) and 11 can then be rewritten as,

$$\beta\frac{\partial^2 C}{\partial X} + \frac{\partial^2 C}{\partial Y} = \frac{\partial C}{\partial T} \qquad [\ 14(a)\ ]$$

$$\gamma\frac{\partial^2 C}{\partial X} + \alpha\frac{\partial^2 C}{\partial Y} = \frac{\partial C}{\partial T} \qquad [\ 14(b)\ ]$$

We now define differential operators

$$\lambda_x = \frac{\partial^2}{\partial X^2} \qquad [\ 15(a)\ ]$$

$$\lambda_y = \frac{\partial^2}{\partial Y^2} \qquad [\ 15(b)\ ]$$

$$\lambda_x' = \frac{\partial}{\partial X} \qquad [\ 15(c)\ ]$$

$$\lambda_y' = \frac{\partial}{\partial X} \qquad [\ 15(d)\ ]$$

such that

$$\lambda = \lambda_x + \lambda_y \qquad [\ 16(a)\ ]$$

and

$$\lambda' = \lambda_x + \lambda_y \qquad [\ 16(b)\ ]$$

The system of differential equations is now readily suseptible to a numerical solution:

Firstly, equation 14(a) can be integrated with respect to time to yield,

$$C(X,Y,T+\delta T) = \exp(\lambda\delta T)C(X,Y,T) \qquad [\ 17\ ]$$

and, multiplying equation 17 by $\exp(-\frac{1}{2}\lambda\delta T)$ to symmetrize, we get,

$$C(X,Y,T+\delta T)\exp(-\tfrac{1}{2}\lambda\delta T) = C(X,Y,T)\exp(\tfrac{1}{2}\lambda T) \qquad [\ 18\ ]$$

which can be expanded, ignoring terms of order $(\delta T)^2$ and higher, to obtain,

$$(1 - \tfrac{1}{2}\lambda\delta T)C(X,Y,T+\delta T) = (1 + \tfrac{1}{2}\lambda\delta T)C(X,Y,T) \qquad [\ 19\ ]$$

The method of Peaceman and Rachford can now be applied to these equations to obtain a system of tridiagonal equations [ 67 ]. The method is a so called alternating direction method (ADI) and it involves the introduction of an artificial intermediate concentration, $C^*(X,Y,T)$.

The numerical scheme requires a suitable grid which is defined as follows:

$$C^n_{i,j} = C(X,Y,T) \qquad [\ 20(a)\ ]$$

where,

$$i = \frac{X}{\delta x} \quad ; \quad j = \frac{Y}{\delta y} \quad ; \quad n = \frac{T}{\delta T} \qquad [\ 20(b,\ c,\ d)\ ]$$

where the i,j represent spacial grid coordinates, and n indicates the n-th time step of length $\delta T$. The grid consists of

13 x 101 spacial elements.

Define $C^*(X,Y,T)$ such that

$$(1 - \tfrac{1}{2}\lambda_x \delta T)C^*(X,Y,T) = (1 + \tfrac{1}{2}\lambda_y \delta T)C(X,Y,T) \qquad [\ 21(a)\ ]$$

$$(1 - \tfrac{1}{2}\lambda_y \delta T)C(X,Y,T) = (1 + \tfrac{1}{2}\lambda_x \delta T)C^*(X,Y,T) \qquad [\ 21(b)\ ]$$

Replacing the differential operators by their corresponding finite difference operators according with

$$\lambda_x C \sim \delta_x^2 C^n_{i,j} = \frac{\beta}{(\delta x)^2}\left[C^n_{i+1,j} - 2C^n_{i,j} + C^n_{i-1,j}\right] \qquad [\ 22(a)\ ]$$

$$\lambda_y C \sim \delta_y^2 C^n_{i,j} = \frac{1}{(\delta y)^2}\left[C^n_{i,j+1} - 2C^n_{i,j} + C^n_{i,j-1}\right] \qquad [\ 22(b)\ ]$$

yields a system of tridiagonal equations of the form

$$AC^{n*}_{i-1,j} + BC^{n*}_{i,j} + AC^{n*}_{i+1,j} = A'C^n_{i,j-1} + B'C^n_{i,j} + A'C^n_{i,j+1} \qquad [\ 23\ ]$$

where ,

$$A = -\frac{\delta T \beta}{2(\delta x)^2} \qquad B = 1 + \frac{\delta T \beta}{2(\delta x)^2} \qquad [\ 24(a)\ ]$$

$$A' = \frac{\delta T}{2(\delta y)^2} \qquad B' = 1 - \frac{\delta T}{2(\delta y)^2} \qquad [\ 24(b)\ ]$$

Similarly, we can obtain a system of equations for the line of grid points, (1,j), by specifying

$$\lambda_x' C^n_{1,j} \sim \delta_x C^n_{1,j} = \frac{\gamma}{\delta_x}\left(C^n_{2,j} - C^n_{1,j}\right) \qquad [\ 25(a)\ ]$$

$$\lambda_y' C^n_{i,j} \sim \delta_y' C^n_{i,j} = \frac{\alpha}{\delta y^2}\left(C^n_{i,j+1} - 2C^n_{i,j} - C^n_{i,j-1}\right) \qquad [\ 25(b)\ ]$$

Note: Equation 25(a) is a 1-sided approximation to the derivative.

The system of equations given by eqn 23 can be written more explicitly as:

$$\begin{aligned}
AC^{n*}_{1,j} + BC^{n*}_{2,j} + AC^{n*}_{3,j} &= A'C^n_{2,j-1} + B'C^n_{2,j} + A'C^n_{2,j+1}\\
AC^{n*}_{2,j} + BC^{n*}_{3,j} + AC^{n*}_{4,j} &= A'C^n_{3,j-1} + B'C^n_{3,j} + A'C^n_{3,j+1}\\
AC^{n*}_{3,j} + BC^{n*}_{4,j} + AC^{n*}_{5,j} &= A'C^n_{4,j-1} + B'C^n_{4,j} + A'C^n_{4,j+1}\\
&\ldots \quad \ldots \quad \ldots \quad \ldots \quad \ldots \quad \ldots\\
&\ldots \quad \ldots \quad \ldots \quad \ldots \quad \ldots \quad \ldots \qquad [\ 26\ ]\\
&\ldots \quad \ldots \quad \ldots \quad \ldots \quad \ldots \quad \ldots\\
AC^{n*}_{99,j} + BC^{n*}_{100,j} + AC^{n*}_{101,j} &= A'C^n_{100,j-1} + B'C^n_{100,j} + A'C^n_{100,j+1}\\
2AC^{n*}_{100,j} + BC^{n*}_{101,j} &= A'C^n_{101,j-1} + B'C^n_{101,j} + A'C^n_{101,j+1}
\end{aligned}$$

A similar system of equations can be obtained for the boundary condition of equation 14(b) which, when combined with equation 26 gives rise to a tridiagonal matrix, the general form of which is given by:

$$
\begin{bmatrix}
B_1T_1 & C_1T_2 & & & & & \\
A_2T_1 & B_2T_2 & C_2T_3 & & & & \\
 & A_3T_2 & B_3T_3 & C_3T_4 & & & \\
 & & \cdot\cdot & \cdot\cdot & \cdot\cdot & & \\
 & & & \cdot\cdot & \cdot\cdot & \cdot\cdot & \\
 & & & & \cdot\cdot & \cdot\cdot & \cdot\cdot \\
 & & & & & A_{M-1}T_{M-2} & B_{M-1}T_{M-1} & C_{M-1}T_M \\
 & & & & & & A_MT_{M-1} & B_MT_M
\end{bmatrix}
=
\begin{bmatrix}
D_1 \\ D_2 \\ D_3 \\ \cdot\cdot \\ \\ \\ \cdot\cdot \\ \cdot\cdot \\ D_{M-1} \\ D_M
\end{bmatrix}
$$

This system of equations can readily be solved using the following recursive scheme:

(i) evaluate $D_i$

(ii) define $W_1$, $Q_1$ such that

$$W_1 = \frac{C_1}{B_1} \qquad [\ 28(a)\ ]$$

$$Q_1 = \frac{D_1}{B_1} \qquad [\ 28(b)\ ]$$

(iii) evaluate remaining $W_i$, $Q_i$ using the recursive relations:

$$W_i = \frac{C_i}{B_i - A_i W_{i-1}} \qquad [\ 29(a)\ ]$$

$$Q_i = \frac{D_i - A_i Q_{i-1}}{B_i - A_i W_{i-1}} \qquad [\ 29(b)\ ]$$

(iv) then,

$$T_M = Q_M \qquad [\ 30\ ]$$

(v) recursively obtain the remaining $T_i$,

$$T_i = Q_i - W_i T_{i+1} \qquad [\ 31\ ]$$

The numerical solution was obtained by using this method according to the scheme described below:

(a) Compute $C^{n*}$ for the grain-boundary; this then allows the computation of

(b) $C^{n*}$ over the lattice part of the grid

This concludes the "forward integration" and this is followed by the "backward integration" which consists of

(c) Evaluate $C^{n+1}$ for the lattice using eqn. 21(b)

(d) Finally, compute $C^{n+1}$ for the grain-boundary

(e) Go to (a) to repeat this process for next $\delta T$

The usefulness of using this computation scheme derives largely from the relaxed constraints on the size of the time step, $\delta T$, which in our case could be from 30-100 times larger than that necessary if an explicit finite difference computation scheme was employed. It was found that using the A.D.I. method of Peaceman and Rachford, that the computation time was reduced from around 5 hours of cpu time, when using an explicit method, to less than 3 minutes.



Results:

A typical set of of profiles are shown in figure A.3. The value of $D_l$ has been kept constant at $4.4 \times 10^{/20}$ $m^2s^{-1}$, while the value of $D_b$ has been varied over a range of 6 orders of magnitude from $1 \times 10^{-19}$ - $1 \times 10^{-13}$ $m^2s^{-1}$. For $D_{g.b} >> D_l$, the shape of the profile resembles the familiar erf function characteristic of lattice diffusion in the region close to the source .However, the profile differs quite radically as the

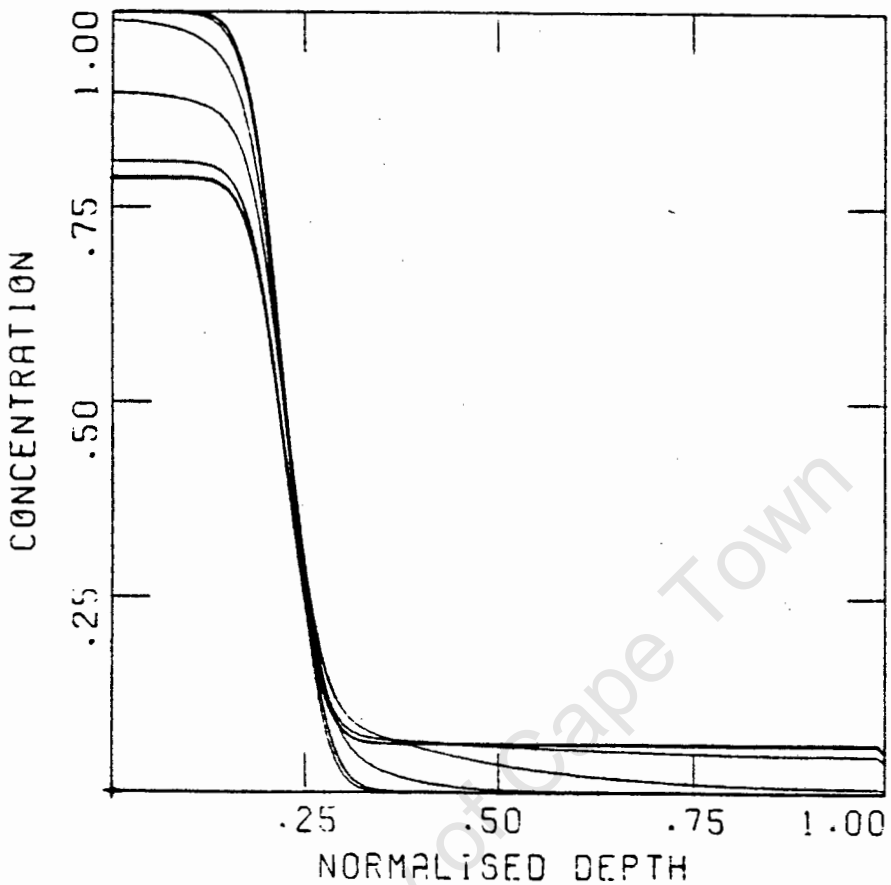


Fig. A.3 Concentration versus depth profile showing the effect of increasing the value of the grain-boundary coefficient while keeping $D_l$ constant. $D_l = 4.4 \times 10^{-20}$; $D_{g.b.} = 10^{-19} - 10^{-13}$ $m^2 s^{-1}$.



distance from the source increases. The profile assumes a linear form as one moves further away from the source region. This type of profile seems reasonable if the grain-boundaries are thought of as high diffusivity channels which act as sources for the lattice.

The results are in qualitative agreement with investigations on similar systems [ 55, 56 ]. An important feature which is

clearly illustrated by fig A.3 is that the amount of material which diffuses into the lattice does not increase linearly with an increase in grain-boundary coefficient. Indeed, the tracer profile asymptotically approaches a constant value as the grain-boundary diffusion coeffient increases. The reason for this behaviour is that as the grain-boundary diffusion coeffient increases, the variation of concentration along the grain boundary approaches zero because the lattice diffusion becomes so slow (relative to the grain-boundary diffusivity) that it becomes the sole factor controlling the exchange of material between grain-boundary and lattice. In other words the material in the grain boundary is always thoroughly intermixed once the diffusivity of this region exceeds the lattice diffusivity by a factor of $\sim 10^4$. This case is particularly relevant for this study because it was found that the experimental profiles could only be fitted if the grain boundary diffusivity was many orders of magnitude larger than the lattice diffusion coefficient. The profile has been found to depend on two other factors viz. the grain-boundary width and, the grain spacing. The variation of these parameters has been investigated but we do not present the results in any detail here. Increasing the grain-boundary width is equivalent to increasing the relevant diffusion coefficient. Increasing the grain spacing resulted in a reduction in the total amount of spreading. It was found that increasing the grain size by ~200Å, necessitated a 2-fold increase in the lattice diffusivity. The reverse was approximately true for a corresponding decrease in the grain size by a similar amount.

The results obtained are in agreement with the results of similar models [ 36, 39, 55 ].

The model has been tested in three ways:

(i) Setting the grain-boundary coefficient equal to the lattice diffusion coefficient reduces the problem to one of pure lattice diffusion. The result is identical with the analytical solution for pure lattice diffusion.

(ii) The model has also been modified slightly for comparison with the work of Gilmer and Farrel. In this case the finite source has been replaced by a constant source at the origin. The results obtained in this case are in agreement with the above authors.

(iii) The self-diffusion data of Botha et al [ 47 ], strongly suggests that grain-boundary diffusion occurs in PtSi and NiSi. Their concentration profiles exibit the "tail" which is apparently characteristic of grain-boundary diffusion. Re-analysis of their data, assuming both lattice diffusion and grain-boundary diffusion, with assumed grain size of 600Å, has yielded the following activation energies. For PtSi: Q = 1.8 eV; Botha finds Q = 2.1eV. Both these results are consistent with metal being the diffusing species (activation energy for growth Q = 1.5eV), under the assumption that the activation energy of transport of the DMS is that energy which determines the activation energy of formation of the silicide.

For NiSi we find Q = 2.2eV which is close to the value reported by Botha (Q = 1.9eV).

## REFERENCES


1. K.N. Tu in Thin Films Interdiffusion and Reactions chapter 10,Edited J.M. Poate, K.N. Tu and J.W. Mayer (John Wiley and Sons, New York, 1978)
2. K.E. Sundstrom, S. Petersson and P.A. Tove, Phys Status Solidi (a)., 20, 653, 1978
3. U. Gosele and K.N. Tu, J. Appl. Phys., 53(4), ,1982
4. G. Ottaviani, J. Vac. Sci. Technol., 16,1112,1979
5. A. Nyland, Acta. Chem. Scand., 20, 2381, 1966
6. K.N. Tu, J. Appl. Phys., 53(1), ,1982
7. H.B. Moffatt, Binary Phase Diagram Handbook,General Electric Company 1976
8. J.M. Poate and T.C.Tisone, Appl. Phys. Letters, 24 (8), , 1974
9. K.N. Tu, G. Ottaviani, R.D. Thompson, J.W. Mayer, J. Appl. Phys.,53(6), , 1982
10. Hutchings and Shepela, Thin Solid Films, 18, 343, 1973
11. Baglin and F. d' Heurle,Thin Solid Films Interactions and Interfaces Editors Baglin and J.M. Poate 1980
12. R. Anderson, J. Baglin, W. Hammer, F. d' Heurle, S.Petersson, Appl. Phys. Letters, 35(3), 285, 1979
13. B.Y. Tsaur, S.S. Lau and J.W. Mayer, Appl. Phys. Letters 35(3), 225, 1979
14. M. von Allmen, S.S. Lau, B.Y. Tsaur, Appl. Phys. Letters, 37(1), 84, 1980

15. B.Y. Tsaur and M-A Nicolet, Appl Phys. Letters, 37(8), 708, 1980

16. H. Langer and E. Wachtel, Z. Metallk., 72, 769, (1981)

17. W-D. Buckley and S.C. Moss, Solid State Electron., 15, 1331,1982

18. N.Cheung, S.S. Lau, M-A Nicolet, J.W. Mayer and T.T. Sheng, in J.E.E. Baglin and J.M. Poate (eds.), Proc. Symp. on Thin Film Interfaces and Interaction, Vol. 80-2, Electrochemical Society, Princeton, N.J.,1980

19. S.S. Lau, D. Sigurd, J. Electrochem. Soc., 121, 1538, 1974

20. E.C. Zingu, Atomic Mobility In Thin Solid Pd2Si Films, Phd Thesis, University of Cape Town, 1985

21. R.W. Bower, D. Sigurd, D.M. Scott, Solid State Electron., 16, 1461, 1973

22. H. Ishiwara, K. Hikosaka, M. Nagatomo and S. Furukawa, Surface Science, 86, 711, 1979

23. D. Sigurd, R.W. Bower, W.F. van der Weg, J.W. Mayer, Thin Solid Films, 19, 319, 1973

24. R.W. Bower and J.W. Mayer, Appl. Phys. Letters, 20,35, 1972

25. D.J. Fertig and G.Y. Robinson, Solid State Electron., 19, 407, 1976

26. N. Cheung, M-A Nicolet, M. Wittmer, C.A. Evans,Jr. and T.T. Sheng, Thin Solid Films, 79, 51, 1981

27. R.W. Bower, D. Sigurd, D.M. Scott, Thin Solid Films, 16,1461,1981

28. F. Foll, P.S. Ho, K.N. Tu, J. Appl. Phys., 52(1), 250, 1981

29. F. Foll and P.S. Ho, J. Appl. Phys. 52(9), 5510, 1981

30. W. K. Chu, H. Krautle, J. W. Mayer, H. Muller and M-A Nicolet, Appl. Phys. Lett., 25, 454, (1974)

31. G. J. van Gurp, W. F. van der Weg and D. Sigurd, J. Appl., Phys., 49, 4011, (1978)

32 R. Pretorius, J. Electrochem. Soc., 128, 107, (1981)

33. W.K. Chu, S.S. Lau, J.W. Mayer, H. Muller and K.N. Tu, Thin Solid Films, 25, 393, 1975

34. R. Pretorius and A. P. Botha, Thin Solid Films, 91, 99, 1982

35. R. Pretorius, C.L. Ramiller and M-A Nicolet, Nucl. Instrum. Methods, 149, 629, 1978

36. K.T. Ho, C-D Lien, U. Shreter, M-A Nicolet, J. Appl. Phys., 57(2), 217, 1485

37. D.M. Scott, M-A Nicolet, Nucl. Instrum. Methods, 209/210, 297, 1983

38. C-D Lien, M-A Nicolet and C.S. Pai, J. Appl. Phys., 57(2), 224, 1985

39. L.S. Hung, J.W. Mayer, C.S. Pai, S.S. Lau, J. Appl. Phys., 58(4), 1527, 1985

40. E.O. Kirkendall, Trans. AIME, 147, 104, 1942

41. A.D. Smigelskas, E.O. Kirkendall, Trans AIME, 171, 130, 1947

42. W.K. Chu, H. Kratle, J.W. Mayer, H. Mller, M-A Nicolet and K.N. Tu, Appl. Phys. Lett., 25, 454, 1974

43. G.T. van Gurp, D. Sigurd and W.F. van der Weg, Appl. Phys. Lett., 29, 159, 1976

44. L.S. Darken, Trans. AIME, 175, 184, 1948

45. G.V. Kidson, J. Nucl. Mater., 3, 21, 1961

46. R. Pretorius, Z.L. Liau, S.S. Lau and M-A Nicolet, Appl. Phys. Lett., 29, 598, 1974

47. A.P. Botha, Solid State Diffusion in metal silicides ,Phd Thesis, University of Stellenbosch, 1982

48. J.R. Manning, Diffusion Kinetics for atoms in crystals, (D van Nostrand Co., Inc. Princeton, New Jersey, 1973)

49. J. Crank, The Mathematics of Diffusion, Oxford University Press, 1975

50. R.E. Hoffmann and D.Turnbull, J.Appl. Phys., 22, 634, 1951

51. J.C. Fisher, J. Appl. Phys., 22, 74, 1951

52. R.T.P. Whipple, Phil. Mag., 45, 1225, 1954

53. A.E. Austin and N.A. Richards, J. Appl. Phys., 33, 3569, 1962

54. Suzuoka, J. Phys. Soc. Jap.,19, 839, 1964

55. G.H. Gilmer and H.H. Farrell, J. Appl. Phys., 47, 3792, 1976

56. G.H. Gilmer and H.H. Farrell, J. Appl. Phys., 47,4373, 1976

57. J. Unnam, J.A. Carpenter, A.R. Houska, J. Appl. Phys., 44, 1957, 1973

58. C. Zener, J. Appl. Phys., 20, 950, 1949

59. C. Wagner, ACTA Metallurgica, 17, 99, 1969

60. S.R. Shatynski, J.P. Hirth, R.A. Rapp, ACTA Metallurgica, 24, 1071,1976

61. G.H. Gilmer and H.H. Farrell, J. Appl. Phys., 45, 4025, 1974

62. U. Gosele, K.N. Tu, J. Appl. Phys., 53, 3252, 1982

63. C-D Lien, M-A Nicolet, J. Appl. Phys., 55, 4187, 1984

64. C-D Lien, J. Appl. Phys., 57(10), 4554, 1985

65. J. E. E. Baglin, H. A. Atwater, D. Gupta and F. M. de'Heurle, Thin Solid films,

66. B. Coulman and H. Chen, J. Appl., Phys., 59(10), 3467, 1986

67. H. Ishiwara, Thin Solid films, 92, 147, 1982

68. A. R. Mitchell, Computational Methods in Partial Differential Equations, Wiley, London, 1969